



**HAL**  
open science

## Persistent Sodium Current Drives Excitability of Immature Renshaw Cells in Early Embryonic Spinal Networks

Juliette Boeri, Hervé Le Corrond, François-Xavier Lejeune, Barbara Le Bras, Christine Mouffle, Monara Kaelle S.C. Angelim, Jean-Marie Mangin, Pascal Branchereau, Pascal Legendre, Antony Czarnecki

► **To cite this version:**

Juliette Boeri, Hervé Le Corrond, François-Xavier Lejeune, Barbara Le Bras, Christine Mouffle, et al.. Persistent Sodium Current Drives Excitability of Immature Renshaw Cells in Early Embryonic Spinal Networks. *Journal of Neuroscience*, 2018, 38 (35), pp.7667-7682. 10.1523/JNEUROSCI.3203-17.2018 . hal-03220695v2

**HAL Id: hal-03220695**

<https://hal.sorbonne-universite.fr/hal-03220695v2>

Submitted on 7 May 2021

**HAL** is a multi-disciplinary open access archive for the deposit and dissemination of scientific research documents, whether they are published or not. The documents may come from teaching and research institutions in France or abroad, or from public or private research centers.

L'archive ouverte pluridisciplinaire **HAL**, est destinée au dépôt et à la diffusion de documents scientifiques de niveau recherche, publiés ou non, émanant des établissements d'enseignement et de recherche français ou étrangers, des laboratoires publics ou privés.

---

**Research Articles: Systems/Circuits**

**Persistent sodium current drives excitability of immature Renshaw cells in early embryonic spinal networks**

Juliette Boeri<sup>a</sup>, Hervé Le Corronc<sup>a,b</sup>, François Xavier Lejeune<sup>a</sup>, Barbara Le Bras<sup>a</sup>, Christine Mouffle<sup>a</sup>, Monara Kaelle S.C. Angelim<sup>a</sup>, Jean Marie Mangin<sup>a</sup>, Pascal Branchereau<sup>c,d</sup>, Pascal Legendre<sup>a</sup> and Antony Czarnecki<sup>a</sup>

<sup>a</sup>INSERM, UMR\_S 1130, CNRS, UMR 8246, Neuroscience Paris Seine, Institute of Biology Paris Seine, 75005 Paris, France. Sorbonne Univ, UPMC Univ Paris 06, UM CR18, 75005 Paris, France.

<sup>b</sup>Univ Angers, 49000 Angers, France.

<sup>c</sup>Bordeaux, INCIA, UMR 5287, F-33615 Pessac, France.

<sup>d</sup>CNRS, INCIA, UMR 5287, F-33615 Pessac, France.

DOI: 10.1523/JNEUROSCI.3203-17.2018

Received: 8 November 2017

Revised: 14 June 2018

Accepted: 29 June 2018

Published: 16 July 2018

---

**Author contributions:** J.B., H.L.C., F.-X.L., B.L.B., M.K.S.A., P.B., P.L.nd A.C. performed research; J.B., H.L.C., F.-X.L., J.M.M., P.B., P.L.nd A.C. analyzed data; J.B., H.L.C., J.M.M., P.B., P.L.nd A.C. wrote the paper; H.L.C., P.B., P.L.nd A.C. designed research; C.M. contributed unpublished reagents/analytic tools.

**Conflict of Interest:** The authors declare no competing financial interests.

We thank Elim Hong for helpful discussion. This work was supported by FRM grant DEQ20160334891, AFM Grant 18564, the Institut National de la Santé et de la Recherche Médicale and the Centre National de la Recherche Scientifique. The authors declare no competing financial interests.

**Correspondence should be addressed to** either of the following: Dr Antony Czarnecki or Dr Pascal Legendre, Institut National de la Santé et de la Recherche Médicale Unité Mixte de Recherche S1130, Centre National de la Recherche Scientifique Unité Mixte de Recherche 8246, Université Pierre et Marie Curie, Bâtiment B, Etage 2, Boîte postale 37, 7 quai Saint Bernard, 75005 Paris, France, E-mail: [antony.czarncki@sorbonne-universite.fr](mailto:antony.czarncki@sorbonne-universite.fr) or [pascal.legendre@inserm.fr](mailto:pascal.legendre@inserm.fr)

**Cite as:** J. Neurosci ; 10.1523/JNEUROSCI.3203-17.2018

**Alerts:** Sign up at [www.jneurosci.org/cgi/alerts](http://www.jneurosci.org/cgi/alerts) to receive customized email alerts when the fully formatted version of this article is published.

Accepted manuscripts are peer-reviewed but have not been through the copyediting, formatting, or proofreading process.

Copyright © 2018 the authors

1 **Persistent sodium current drives excitability of immature Renshaw cells in**  
2 **early embryonic spinal networks**

3  
4 **Abbreviated title:**  $I_{\text{Nap}}$  drives the excitability of newborn V1<sup>R</sup>

5  
6  
7 **Juliette Boeri**<sup>a,1</sup>, **Hervé Le Corrond**<sup>a,b,1</sup>, **François Xavier Lejeune**<sup>a</sup>, **Barbara Le Bras**<sup>a</sup>,  
8 **Christine Mouffle**<sup>a</sup>, **Monara Kaelle S.C. Angelim**<sup>a</sup>, **Jean Marie Mangin**<sup>a</sup>, **Pascal**  
9 **Branchereau**<sup>c,d</sup>, **Pascal Legendre**<sup>a,1</sup>, **Antony Czarnecki**<sup>a,1</sup>

10  
11 <sup>a</sup> INSERM, UMR\_S 1130, CNRS, UMR 8246, Neuroscience Paris Seine, Institute of Biology  
12 Paris Seine, 75005 Paris, France. Sorbonne Univ, UPMC Univ Paris 06, UM CR18, 75005  
13 Paris, France.

14 <sup>b</sup> Univ Angers, 49000 Angers, France.

15 <sup>c</sup> Univ. Bordeaux, INCIA, UMR 5287, F-33615 Pessac, France.

16 <sup>d</sup> CNRS, INCIA, UMR 5287, F-33615 Pessac, France.

17  
18 Correspondence should be addressed to either of the following: Dr Antony Czarnecki or Dr  
19 Pascal Legendre, Institut National de la Santé et de la Recherche Médicale Unité Mixte de  
20 Recherche S1130, Centre National de la Recherche Scientifique Unité Mixte de Recherche  
21 8246, Université Pierre et Marie Curie, Bâtiment B, Etage 2, Boîte postale 37, 7 quai Saint  
22 Bernard, 75005 Paris, France, E-mail: antony.czarnecki@sorbonne-universite.fr or  
23 pascal.legendre@inserm.fr.

24  
25 **Number of pages:** 38

26  
27 **Number of figures:** 10

28  
29 **Number of tables:** 2

30  
31 **Number of words:**

32 Abstract: 250

33 Introduction: 641

34 Discussion: 1492

35  
36 **Acknowledgements:**

37 We thank Elim Hong for helpful discussion. This work was supported by FRM grant  
38 DEQ20160334891, AFM Grant 18564, the Institut National de la Santé et de la Recherche  
39 Médicale, and the Centre National de la Recherche Scientifique. The authors declare no  
40 competing financial interests.

41 <sup>1</sup>J. B., H. L., P. L. and A. C. contributed equally to this work.

42

43 **ABSTRACT**

44

45 Spontaneous network activity (SNA) emerges in the spinal cord (SC) before the formation of  
46 peripheral sensory inputs and central descending inputs. SNA is characterized by recurrent  
47 giant depolarizing potentials (GDPs). Because GDPs in motoneurons (MNs) are mainly  
48 evoked by prolonged release of GABA, they likely necessitate sustained firing of  
49 interneurons. To address this issue we analyzed, as a model, embryonic Renshaw cell ( $V1^R$ )  
50 activity at the onset of SNA (E12.5) in the embryonic mouse SC (both sexes).  $V1^R$  are one of  
51 the interneurons known to contact MNs, which are generated early in the embryonic SC.  
52 Here, we show that  $V1^R$  already produce GABA in E12.5 embryo, and that  $V1^R$  make  
53 synaptic-like contacts with MNs and have putative extrasynaptic release sites, while paracrine  
54 release of GABA occurs at this developmental stage. In addition, we discovered that  $V1^R$  are  
55 spontaneously active during SNA and can already generate several intrinsic activity patterns  
56 including repetitive-spiking and sodium-dependent plateau potential that rely on the presence  
57 of persistent sodium currents ( $I_{NaP}$ ). This is the first demonstration that  $I_{NaP}$  is present in the  
58 embryonic SC and that this current can control intrinsic activation properties of newborn  
59 interneurons in the SC of mammalian embryos. Finally, we found that 5  $\mu$ M riluzole, which is  
60 known to block  $I_{NaP}$ , altered SNA by reducing episode duration and increasing inter-episode  
61 interval. Because SNA is essential for neuronal maturation, axon pathfinding and  
62 synaptogenesis, the presence of  $I_{NaP}$  in embryonic SC neurons may play a role in the early  
63 development of mammalian locomotor networks.

64 **SIGNIFICANCE STATEMENT**

65 The developing spinal cord (SC) exhibits spontaneous network activity (SNA) involved in the  
66 building of nascent locomotor circuits in the embryo. Many studies suggest that SNA depends  
67 on the rhythmic release of GABA, yet intracellular recordings of GABAergic neurons have  
68 never been performed at the onset of SNA in the SC. We first discovered that embryonic  
69 Renshaw cells ( $V1^R$ ) are GABAergic at E12.5 and spontaneously active during SNA. We  
70 uncover a new role for persistent sodium currents ( $I_{NaP}$ ) in driving plateau potential in  $V1^R$   
71 and in SNA patterning in the embryonic SC. Our study thus sheds light on a role for  $I_{NaP}$  in  
72 the excitability of  $V1^R$  and the developing SC.

73

74 **INTRODUCTION**

75 A remarkable feature of the developing central nervous system (CNS) is its capacity to  
76 generate spontaneous network activity (SNA) at the end of neuronal migration. SNA occurs in  
77 the absence of any external inputs and is not experience-driven or use-dependent (Moody,  
78 1998; Feller, 1999). SNA has been described as playing an essential role in several areas of  
79 the developing CNS, including the neocortex, the thalamus, the hippocampus, the locus  
80 coeruleus, the retina and the spinal cord (Landmesser and O'Donovan, 1984; Ben-Ari et al.,  
81 1989; Garaschuk et al., 1998; Feller, 1999; Garaschuk et al., 2000; Gust et al., 2003; Corlew  
82 et al., 2004; Marder and Rehm, 2005; Myers et al., 2005; Gonzalez-Islas and Wenner, 2006;  
83 Hanson et al., 2008; Rockhill et al., 2009; Watt et al., 2009). SNA regulates the development  
84 of neural circuits by influencing synaptogenesis, neuronal maturation, axonal guidance and  
85 axonal pathfinding (Zhang and Poo, 2001; Hanson et al., 2008; Kirkby et al., 2013).

86 In the embryonic spinal cord (SC), SNA is characterized by long-lasting bursts of action  
87 potentials (APs) occurring every 2-4 min that can propagate along the cord (Hanson and  
88 Landmesser, 2003). SNA occurs at the onset of synaptogenesis at E12.5, before the  
89 emergence of functional neuromuscular junction and the formation of sensory and supra-  
90 spinal inputs (Hanson and Landmesser, 2003). Bursts of APs recorded on ventral roots  
91 (Hanson and Landmesser, 2003) or in the whole SC (Yvert et al., 2004) are long-lasting  
92 episodes characterizing SNA in the embryonic SC. We previously showed that most  
93 individual motoneurons (MNs) only generate a single AP during each episode of SNA  
94 (Czarnecki et al., 2014) and we demonstrated that acetylcholine (ACh) release could not  
95 directly synchronize MN firing during SNA as MNs do not express functional acetylcholine  
96 receptors (Czarnecki et al., 2014). Therefore, MNs must rely on other mechanisms to  
97 synchronize their firing during SNA. We have recently shown that MN activity occurring  
98 during SNA at the onset of synaptogenesis (E12.5) is generated by giant depolarizing  
99 potentials (GDPs) involving a massive and long-lasting release of GABA, as well as a

100 moderate release of glutamate and glycine (Czarnecki et al., 2014). It is therefore likely that  
101 newborn GABAergic interneurons (INs) play an essential role in the generation of the  
102 sustained episodes of depolarization necessary to synchronize MN firing during SNA.

103 To gain insight into the excitability pattern of spinal GABAergic INs involved in the  
104 release of GABA during SNA, we used multiple approaches to examine the intrinsic  
105 activation properties of immature Renshaw cells ( $V1^R$ ) in the lumbar SC. Renshaw cells are  
106 known to regulate MN activity in the adult through recurrent synaptic inhibition (Eccles et al.,  
107 1956) and play an important role in the regulation of SC activity at late developmental stages  
108 in the chicken embryo (Wenner and O'Donovan, 2001).  $V1^R$  are the first V1 INs to be  
109 generated during neurogenesis in the mouse embryo (Benito-Gonzalez and Alvarez, 2012).  
110 From E9.5 to E12.5,  $V1^R$  migrate toward their final location between MN columns and the  
111 ventrolateral funiculus (Benito-Gonzalez and Alvarez, 2012; Alvarez et al., 2013). Because  
112 glycine, unlike GABA, is nearly absent in SC INs of E12.5 mouse embryo (Allain et al.,  
113 2004, 2006; Scaini et al., 2010),  $V1^R$  are likely to be GABAergic neurons at the early  
114 developmental stage.

115 Here, we show that, like MNs,  $V1^R$  display GDPs during SNA at E12.5. However, we  
116 discovered that, unlike MNs, most  $V1^R$  are able to produce repetitive spiking or sodium-  
117 dependent plateau potentials in response to GDPs (Czarnecki et al., 2014). Remarkably, these  
118 sustained discharges depend on the presence of a persistent sodium current ( $I_{Nap}$ ). In addition,  
119 we also demonstrate that  $I_{Nap}$  already has important functions at the onset of SNA. Inhibition  
120 of  $I_{Nap}$  alters SNA episode duration and inter-episode interval duration, which reveals that the  
121 ability of embryonic SC neurons to generate sustained discharge is required for a correct SNA  
122 pattern (Hanson and Landmesser, 2006).

123

124 **MATERIALS AND METHODS**125 ***Isolated spinal cord preparation***

126       These experiments were performed in accordance with European Community guiding  
127 principles on the care and use of animals (86/609/CEE, CE Off J no. L358, 18 December  
128 1986), French decree no. 97/748 of October 19, 1987 (J Off République Française, 20  
129 October 1987, pp. 12245-12248) and recommendations from the CNRS. We used  
130 GAD67eGFP knock-in mice to visualize putative GABAergic INs (Tamamaki et al., 2003).  
131 Briefly, a cDNA encoding enhanced GFP (eGFP) was targeted to the locus encoding the gene  
132 Gad1. GAD67 is a rate-limiting enzyme of GABA biosynthesis and is known to be a marker  
133 for GABAergic neurons (Le Corrionc et al. 2011). To obtain E12.5 GAD67-eGFP embryos, 8-  
134 to 12-week-old wild-type Swiss female mice were crossed with heterozygous GAD67-eGFP  
135 Swiss male mice. HB9-eGFP mouse embryos were used to visualize MNs (Wichterle et al.,  
136 2002). To obtain E12.5 transgenic HB9-eGFP embryos, 8- to 12-week-old wild-type Swiss  
137 female mice were crossed with heterozygous HB9-eGFP C57BL/6Jrj male mice.

138       269 embryos obtained from 152 pregnant mice were used. Isolated embryonic mouse  
139 SCs were obtained as previously described (Delpy et al., 2008; Scaini et al., 2010). Briefly,  
140 pregnant mice were anesthetized by intramuscular injection of a mix of ketamine and xylazine  
141 and sacrificed using a lethal dose of CO<sub>2</sub>. Embryos of either sex were removed and the SC  
142 was isolated from eGFP-positive embryos. Whole SCs were maintained in an artificial  
143 cerebrospinal fluid (ACSF) containing 135 mM NaCl, 25 mM NaHCO<sub>3</sub>, 1 mM NaH<sub>2</sub>PO<sub>4</sub>, 3  
144 mM KCl, 11 mM glucose, 2 mM CaCl<sub>2</sub>, and 1 mM MgCl<sub>2</sub> (307 mosmol/kg H<sub>2</sub>O),  
145 continuously bubbled with a 95% O<sub>2</sub>-5% CO<sub>2</sub> gas mixture.

146

147 ***Whole-cell recordings and analysis***

148       The isolated SC was placed in a recording chamber and continuously perfused (2  
149 mL/min) at room temperature (20-24°C) with the oxygenated ACSF described above. Whole-



150 cell patch-clamp recordings of lumbar spinal V1<sup>R</sup> and MNs were carried out under direct  
151 visualization using an infrared-sensitive CCD video camera.

152 In the SC of GAD67eGFP mouse embryos, eGFP neurons were detected using UV  
153 light. MNs were identified by their size, their location in the ventral area of the SC  
154 parenchyma (Czarnecki et al., 2014) and by the lack of eGFP expression. These neurons  
155 localized in this SC area express the MN transcription factors *Islet1/2*, as shown in a previous  
156 study (Scain et al, 2010). Recorded eGFP interneurons were localized in the ventrolateral area  
157 of the SC at the marginal zone between motor columns and the ventral funiculus, which is the  
158 known location of developing V1<sup>R</sup> (Stam et al., 2012). To confirm V1<sup>R</sup> identity, recorded  
159 cells were filled with neurobiotin (0.5-1 mg/mL) and stained with an antibody directed against  
160 Foxd3. Foxd3 is a specific transcription factor of V1 INs (Dottori et al., 2001; Stam et al.,  
161 2012) and the hallmark of V1<sup>R</sup> localized in the ventrolateral area of the embryonic SC (Carr et  
162 al., 1998; Benito-Gonzalez and Alvarez, 2012).

163 Whole-cell patch-clamp electrodes were pulled from thick-wall borosilicate glass using  
164 a Brown-Flaming puller (Sutter Instrument Co., USA). The tip of the electrode was fire-  
165 polished using a microforge (Narishige, Japan). Patch-clamp electrodes had resistances of 4-7  
166 M $\Omega$ . The electrode was filled with a solution containing (in mM): 96.4 K methanesulfonate,  
167 33.6 KCl, 4 MgCl<sub>2</sub>, 4 Na<sub>2</sub>ATP, 0.3 Na<sub>3</sub>GTP, 10 EGTA, and 10 HEPES (pH 7.2; 290  
168 mosmol/kg-H<sub>2</sub>O). Using these potassium methanesulfonate solutions, the equilibrium  
169 potential for chloride ions (E<sub>Cl</sub>)  $\approx$  -30 mV was close to the physiological values measured at  
170 E12.5 on spinal MNs (Delpy et al., 2008). The junction potential (6.6 mV) was systematically  
171 corrected offline. In some voltage-clamp experiments, the electrode contained: (in mM) 130  
172 CsCl, 4 MgCl<sub>2</sub>, 4 Na<sub>2</sub>ATP, 10 EGTA and 10 HEPES (pH 7.2; 290 mosmol/kg-H<sub>2</sub>O).

173 Signals were recorded using Axopatch 200B or Multiclamp 700B amplifiers (Molecular  
174 Devices, USA). Data were low-pass filtered (2 kHz), digitized (20 kHz) online using a  
175 Digidata 1440A interface and acquired using PClamp 10.5 software ([pClamp](#),

176 RRID:SCR\_011323). Analyses were performed off-line using PClamp 10.5 software and  
177 Axograph X.1.6.4 (Axograph, RRID:SCR\_014284).

178 In voltage-clamp or current-clamp experiments, neurons were recorded at a holding  
179 potential ( $V_h$ ) of -60 mV. Series resistance (10-20 M $\Omega$ ) was monitored throughout the  
180 experiments and was 50-80% compensated. Data were discarded if series resistance varied by  
181 more than  $\approx$  30% from the initial value. In current-clamp mode,  $V1^R$  intrinsic discharge  
182 patterns were elicited using depolarizing current steps (from 0 to  $\approx$  50 pA, 2-10 pA  
183 increments depending on the input resistance of the cell, 2 seconds) or depolarizing current  
184 triangular-ramp (from 0 to  $\approx$  50 pA, 5 pA increments, 20 seconds) with an 8-second interval  
185 to ensure that the membrane potential returned to baseline  $V_h$ . In voltage-clamp mode, whole-  
186 cell currents were elicited by a depolarizing voltage ramp. The 70 mV/s speed was chosen to  
187 elicit and measure persistent inward currents ( $I_{Nap}$ ) (Huang and Trussell, 2008). Subtraction of  
188 the current evoked by the voltage ramp in the presence of 1  $\mu$ M TTX to control voltage ramp-  
189 evoked current revealed  $I_{Nap}$ .

190 Action potentials or plateau potentials were analyzed based on the following parameters  
191 during a 2-second current step: threshold potential, peak amplitude, half amplitude duration,  
192 rate of rise of events (by dividing the amplitude of the event by the duration from its onset to  
193 the peak; 2 seconds step width).

194 Boltzmann functions were used to describe  $I_{Nap}$  activation on current evoked by voltage  
195 ramp. For the fit current (20 kHz sampling 2 KHz filter):

196

$$197 \quad G = G_{MAX}/(1+\exp(-(V-V_{HALF})/k))$$

198

199 where  $G$  is conductance in nS,  $G_{Max}$  is the maximal conductance,  $V$  is the potential in mV,  
200  $V_{HALF}$  is the voltage for half-maximal activation in mV, and  $k$  is the slope factor in mV.

201 Threshold for activation  $I_{Nap}$  was determined by eye from Boltzmann curves.

202

203 ***Extracellular recordings***

204 In the same experimental conditions as for whole-cell recordings, spontaneous activity  
205 was recorded extracellularly from E12.5 SCs using glass electrodes. Extracellular electrodes  
206 were placed under visual control on the superficial part of the ventral horn both at the cervical  
207 and the lumbar levels. Targeted networks likely include MNs as well as surrounding INs  
208 (Czarnecki et al., 2014). Electrodes were connected to a high-gain a.c. amplifier (ISO-  
209 DAM8A-4 Bio-amplifier System, World Precision Instruments Ltd, Stevenage, UK). Filtered  
210 (Filter cutoff frequency: 0.3-3 kHz) raw signals were integrated off-line and analyzed using  
211 Spike2 software ([Spike2 Software](#), RRID:SCR\_000903). Changes in burst duration and  
212 maximum instantaneous frequency were calculated from cervical and lumbar recordings.

213

214 ***Pharmacological agents***

215 During patch-clamp recordings, drugs were applied using 0.5 mm diameter quartz  
216 tubing positioned 50  $\mu\text{m}$  away from the recording area under direct visual control. The quartz  
217 tubing was connected using a manifold to 6 solenoid valves linked with 6 reservoirs.  
218 Solutions were gravity-fed into the quartz tubing. Drug application was controlled using a  
219 VC-8 valve controller (Warner Instruments, USA). The following pharmacological agents  
220 were used: tetrodotoxin (TTX) (1  $\mu\text{M}$ , Alomone, Israel) and riluzole (5-10  $\mu\text{M}$  Tocris  
221 Bioscience, UK). Both were dissolved in the bath solution.

222

223 ***Immunohistochemistry***

224 All primary antibodies used and their respective dilutions are listed in Table 1. E12.5  
225 embryos were collected from pregnant females. Once dissected out of their yolk sac, these  
226 embryos were immediately immersion-fixed in phosphate buffer (PB 0.12 M) with 4%  
227 paraformaldehyde (PFA; freshly prepared in PB, pH 7.4) for 1 h at 4°C. Embryos were then

228 rinsed with PB and cryoprotected in PB-15% sucrose at 4°C for 24 h and then in PB-30%  
229 sucrose at 4°C for 24 h. Embryos were embedded in OCT medium (VWR, Fontenay-sous-  
230 Bois, France) and quickly frozen. Serial sections 20 µm thick were collected onto slides using  
231 a cryostat. Immunostaining was processed on SC transverse sections and on whole SC post-  
232 recording to confirm IN identity. To reveal neurobiotin-labeled cells, SCs were fixed for 1 h  
233 in 4% PFA and were then incubated in 0.12 M PB at 4°C until immunohistochemical studies.  
234 Tissues (embryo slices and whole SC) were thawed at room temperature, washed in PBS,  
235 incubated in NH<sub>4</sub>Cl (50 mM) diluted in PBS for 20 min and then permeabilized for 30 min in  
236 a blocking solution (10% goat serum in PBS) with 0.2% Triton X-100 and then for 48 h at  
237 4°C with the primary antibodies, which were diluted in the 0.2% Triton X-100 blocking  
238 solution. Slices or whole SCs were then washed in PBS and incubated for 2 h at RT in the  
239 secondary antibodies (diluted at 1/1000 in the 0.2% Triton X-100 blocking solution): Alexa  
240 Fluor 405 (Thermo Fisher Scientific Cat# A-31556, RRID:AB\_221605) or 647 goat anti-  
241 rabbit (Thermo Fisher Scientific Cat# A-21244, RRID:AB\_2535812); Alexa Fluor 594 goat  
242 anti-guinea pig (Thermo Fisher Scientific Cat# A-11076, RRID:AB\_2534120); Alexa Fluor  
243 649 donkey anti-guinea pig (Jackson ImmunoResearch Labs Cat# 706-605-148,  
244 RRID:AB\_2340476); Alexa Fluor 594 goat anti-mouse (Thermo Fisher Scientific Cat# A-  
245 11005, RRID:AB\_2534073); Alexa Fluor 488 goat anti-chicken (Thermo Fisher Scientific  
246 Cat# A-11039, RRID:AB\_2534096) and streptavidin-conjugated Alexa Fluor 405 (1:1000,  
247 Thermo Fisher Scientific Cat# S32351). After washing in PBS, slides or whole SCs were  
248 dried and mounted in Mowiol medium (Millipore, Molsheim, France).

249

### 250 *Confocal microscopy and image analysis*

251 Preparations were analyzed using a Leica SP5 confocal microscope. Immunostaining  
252 was observed using a 40X oil-immersion objective with a numerical aperture of 1.25, as well  
253 as with a 63X oil-immersion objective with a numerical aperture of 1.32 and a 4X digital

254 zoom magnification. Serial optical sections were obtained with a Z-step of 1  $\mu\text{m}$  (40X) and  
255 0.2-0.3  $\mu\text{m}$  (63X). Images (1024x1024; 12-bit color scale) were stored using Leica software  
256 LAS-AF and analyzed using ImageJ 1.5 softwares ([Wright Cell Imaging Facility](#),  
257 RRID:SCR\_008488). Colocalization of synaptophysin staining with calbindin staining, eGFP  
258 staining (MNs; HB9eGFP mouse embryos) or neurobiotin staining was assessed in 3 axes  
259 using a single confocal slice and X and Y orthogonal views of the stack (ImageJ 1.5).

260

261 ***Sniffer recordings.***

262 To make a “sniffer” electrode (Young and Poo, 1983) for GABA, an outside-out patch  
263 was pulled from a transfected HEK293 cell line expressing the GABA<sub>A</sub>R subunits  $\alpha 3\beta 2\gamma 2$   
264 (kindly provided by Michel Partiseti, Sanofi Advantis R&D LGCR/LIT, France). This  
265 GABA<sub>A</sub>R is highly specific for GABA and is characterized by slow desensitization, which  
266 makes it a good sensor for GABA paracrine release (Barberis et al., 2007). As a control, the  
267 electrode was first positioned outside the SC to verify any GABA contamination in the  
268 recording medium. The electrode was then pushed inside the SC and positioned within the  
269 motoneuronal area and the ventral funiculi. Outside-out patch-clamp electrodes (5-10 M $\Omega$ )  
270 were pulled from thick-wall borosilicate glass, fire-polished and filled with (in mM): CsCl  
271 130, MgCl<sub>2</sub> 4, Na<sub>2</sub>ATP 4, EGTA 10, HEPES 10 (pH 7.2, osmolarity 290 mosmol/kg-H<sub>2</sub>O).  
272 Single channel currents were recorded using an Axopatch 200B amplifier (Molecular  
273 Devices, USA). Recordings were filtered at 10 kHz, sampled at 50 kHz and stored on a PC  
274 computer. Membrane potential was held at -50 mV throughout the experiment. Analysis of  
275 the sniffer currents was performed using Axograph X.1.6.4 software.

276 Human embryonic kidney 293 cells (HEK293) were maintained in a 95% air - 5% CO<sub>2</sub>  
277 humidified incubator, at 35°C, in Dulbecco’s modified Eagle’s medium supplemented with  
278 0.11 g/L sodium pyruvate, 6 g/L D-glucose, 10% (v/v) heat-inactivated fetal bovine serum (all  
279 from Gibco BRL). Cells were passaged every 5-6 days (up to maximum 20 times). For

280 electrophysiological recordings, cells were seeded onto glass coverslips coated with poly-L-  
281 ornithine (0.1 mg/mL).

282 ***Statistics***

283 All values were expressed as mean  $\pm$  standard deviation. Statistical significance was  
284 assessed by the non-parametric Kruskal-Wallis test with Dunn's post tests, Mann-Whitney  
285 test and Wilcoxon matched pairs test (GraphPad Prism 5.0 Software, USA). Significance was  
286 determined as  $P < 0.05$  (\*),  $P < 0.01$  (\*\*) or  $P < 0.001$  (\*\*).

287 **RESULTS**288 *V1<sup>R</sup> are identified with calbindin, Foxd3 and MafB at the onset of SNA.*

289 In the present study, we used GAD67-enhanced green fluorescent protein (eGFP)  
290 knock-in mice (Tamamaki et al., 2003) to visualize putative GABAergic INs (Figures 1A1,  
291 1B1 and 1C1). V1<sup>R</sup> can be unambiguously identified by their characteristic position in the  
292 ventral horn both in the adult (Geiman et al., 2000) and in the embryo (Sapir et al., 2004;  
293 Stam et al., 2012). Most V1<sup>R</sup> were localized between the ventral border of MN columns and  
294 the ventral funiculi. To identify V1<sup>R</sup> in the lumbar SC of E12.5 GAD67eGFP embryos, we  
295 first performed immunostaining using anti-calbindin, anti-Foxd3 and anti-MafB antibodies  
296 (Figure 1). Calbindin is a calcium-binding protein exclusively expressed by V1<sup>R</sup> when  
297 looking in the ventrolateral area of the SC between the MN columns and the funiculus (Stam  
298 et al., 2012). The forkhead transcription factor Foxd3 controls the early phase of V1<sup>R</sup>  
299 differentiation, whereas MafB is required to maintain V1<sup>R</sup> at later developmental stages, and  
300 both are therefore expressed at E12.5 in V1<sup>R</sup> (Stam et al., 2012). At E12.5 INs located in the  
301 ventrolateral marginal zone between the motor columns and the ventral funiculi express  
302 Foxd3 (Figures 1A2, 1B2 and 1C2) and calbindin (Figures 1A3 and 1B3), as previously  
303 described (Stam et al., 2012; Benito-Gonzalez et al, 2012). Foxd3<sup>+</sup> INs were also observed in  
304 neurons positioned dorsally to the motor columns (Figures 1A2 and 1B2). However, these INs  
305 were not stained by calbindin antibody, hence this population of INs was not included in our  
306 study. In the V1<sup>R</sup> area, double immunostaining (Figures 1A4 and 1B4) indicated that 81.7 ±  
307 15.0% of Foxd3<sup>+</sup> INs localized in the ventral marginal zone were also immunoreactive to  
308 calbindin at E12.5 (n=4 embryos, 2 sections/embryo). To ensure that all Foxd3<sup>+</sup> INs localized  
309 in the area are V1<sup>R</sup>, we performed double immunostaining using anti-Foxd3 and anti-MafB  
310 antibodies (Figures 1C). We found that 100% of Foxd3<sup>+</sup> eGFP<sup>+</sup> INs localized in the ventral  
311 marginal zone were also immunoreactive to anti-MafB antibody (n = 4 embryos, 2  
312 sections/embryo), thus confirming their V1<sup>R</sup> fate (Figure 1C4). It should also be noted that at

313 this developmental stage we detected MafB<sup>+</sup> eGFP<sup>-</sup> neurons localized within the motor  
314 columns (Figures 1C1 and 1C3) that are likely MNs (Stam et al., 2012). Therefore, we used  
315 Foxd3 immunostaining to confirm that the recorded IN belonged to the V1<sup>R</sup> population  
316 (Figures 1D1, 1D2, 1D3 and 1D4). Whereas Calbindin is a good marker for V1<sup>R</sup>, it was not  
317 used to identify recorded V1<sup>R</sup> because of cytoplasm-calbindin dilution complications during  
318 whole-cell recording (Muller et al., 2005), caused by the high nucleus/cytoplasm volume ratio  
319 in embryonic neurons.

320

321 ***V1<sup>R</sup> already produce GABA at E12.5.***

322 As calbindin is localized within the cytoplasm of V1<sup>R</sup>, we used calbindin  
323 immunostaining to visualize V1<sup>R</sup> morphology (Stam et al., 2012).  $96.6 \pm 7.2\%$  of calbindin<sup>+</sup>  
324 neurons in the ventrolateral marginal zone were also eGFP<sup>+</sup> in E12.5 GAD67eGFP knock-in  
325 mouse embryos (n = 4 embryos, 2 sections/embryo), which could suggest that most V1<sup>R</sup> are  
326 likely to produce GABA at this developmental stage. To determine to what extent V1<sup>R</sup> already  
327 produce GABA at E12.5, we performed double immunostaining using anti-calbindin and anti-  
328 GABA antibodies (Figures 2A and 2B). We found that  $90.1 \pm 10.5\%$  (n = 8 embryos, 2  
329 sections/embryo) of calbindin<sup>+</sup> INs localized in the ventrolateral marginal zone (Figures 2A2  
330 and 2B2) were also immunoreactive to GABA antibody (Figures 2A3, 2A4, 2B3 and 2B4),  
331 suggesting that V1<sup>R</sup> already produced enough GABA to be detected by  
332 immunohistochemistry at E12.5.

333 It is important to note that many eGFP<sup>+</sup> GABA<sup>-</sup> INs were detected within the ventral  
334 parenchyma at E12.5, as previously observed (Allain et al., 2004). This could result from the  
335 production of the GAD67 splice variant GAD25. At early developmental stages, GAD1 first  
336 encodes the truncated 25-kDa leader (GAD25) without GAD enzymatic activity and then the  
337 enzymatically active protein GAD44 (see for review (Le-Corronc et al., 2011)). These two  
338 GAD isoforms are down-regulated during neuronal differentiation concomitantly with up-



339 regulation of GAD67 expression.

340

341 ***Synaptic-like contacts are detected between  $V1^R$  and MNs at the onset of SNA***

342 At E12.5,  $V1^R$  axons are localized in ventral funiculi and extend for a few segments  
343 without forming collateral branches entering the motor columns (Alvarez et al., 2013). The  
344 first evidence for collateral  $V1^R$  axons innervating the soma of lumbar MNs was found at  
345 E15.5 only while synaptic-like connections from MNs onto the  $V1^R$  cell body were already  
346 observed at E12.5 (Alvarez et al., 2013). Accordingly, it was proposed that MNs can control  
347  $V1^R$  activity at E12.5 while  $V1^R$  are unable to control MN activity at this time point (Alvarez  
348 et al., 2013). However, it should be noted that synaptophysin staining was found mainly in the  
349 ventral funiculus at E12.5 (Figure 3A1) (Alvarez et al., 2013; Czarnecki et al., 2014), where  
350 IN axonal projections and MN dendrite-like processes were observed (Czarnecki et al., 2014).  
351 Accordingly, we hypothesized that  $V1^R$  already make some synaptic-like contacts with MN  
352 projections within the ventral funiculus.

353 To address this issue we first performed multiple immunostaining using anti-synaptophysin  
354 antibody (putative release site), anti-calbindin antibody ( $V1^R$ ) and anti-eGFP antibody on  
355 coronal sections of the SC HB9eGFP mouse embryos to visualize MNs (Figures 3A2, 3A3,  
356 3A4, 3B1, 3B2 and 3B3). As shown in Figure 3B3, many calbindin<sup>+</sup> fibers were apposed to  
357 MN neurites (eGFP staining) within the ventral funiculus. We found  $21.7 \pm 8.4$   
358 synaptophysin<sup>+</sup> punctates within calbindin<sup>+</sup> fibers apposed to MN neurites per hemi section in  
359 coronal slices (n = 9; 5 embryos) (Figures 3B1, 3B2 and 3B3; inserts, arrow). Conversely,  
360 synaptophysin punctates were also found in MN fibers (eGFP<sup>+</sup>) apposed to calbindin<sup>+</sup> fibers  
361 (Figures 3B1, 3B2 and 3B3; insert, arrow head), which indicate the presence of MN putative  
362 release sites apposed to  $V1^R$  within the ventral funiculus. We also found synaptophysin  
363 punctates within calbindin<sup>+</sup> fibers that were not apposed to MN neurites (Figures 3B1, 3B2  
364 and 3B3; barred arrow). This may indicate the presence of non-synaptic release sites and/or

365 that  $V1^R$  can make contact with fibers of neurons other than MNs. To further confirm the  
366 presence of  $V1^R$  synaptic-like contacts on MNs, we performed multiple immunostaining using  
367 anti-synaptophysin antibody (putative release site) and anti-eGFP antibody on isolated SC  
368 after patch-clamp injection of neurobiotin in  $V1^R$  (Figures 3C). Recorded INs (eGFP negative)  
369 in eGFP HB9 embryos were identified as  $V1^R$  using Foxd3 immunostaining (Figure 3C1;  
370 insert). We found 3 to 5 putative release sites per  $V1^R$  ( $n = 4$  cells) that were apposed to MN  
371 fibers within the ventral funiculus (Figures 3C1, 3C2, 3C3 and 3C4). We did not find any  
372 release site within the  $V1^R$  axonal growth cone (data not shown).

373

374 ***Paracrine release of GABA occurred in the SC of E12.5 mouse embryos.***

375 Paracrine release of GABA may occur from non-synaptic release sites and/or may  
376 reflect neurotransmitter spillover of GABA from immature synapses (Safiulina and  
377 Cherubini, 2009). Therefore, we hypothesized that GABA release can occur at this  
378 developmental stage. To detect the presence of GABA paracrine release, we used the sniffer  
379 technique (Scain et al., 2010). Outside-out patches from HEK cells expressing the  $GABA_A$ R  
380 subunits  $\alpha 3\beta 2\gamma 2$  were used as a “sniffer” to detect the presence of GABA in the extracellular  
381 space (Figure 4 A1). When inserting the sniffer electrode in the vicinity of MNs, we did not  
382 detect any  $GABA_A$ R, thus indicating that basal GABA concentration is below the detection  
383 threshold of the sniffer patch (data not shown). The possibility of evoking GABA release, and  
384 hence  $GABA_A$ R activation, by inducing a global cell membrane depolarization was tested  
385 using bath application of 30 mM KCl (Scain et al., 2010; Czarnecki et al., 2014). Increasing  
386  $[K^+]_o$  evoked a significant  $GABA_A$ R activation in the sniffer patch ( $n = 9$ ), indicating that  
387 GABA can be released in the extracellular space in response to cell membrane depolarization  
388 (Figure 4 A1). We estimated the concentration of released GABA around MNs by comparing  
389 the peak amplitude of the sniffer response evoked by KCl application to sniffer responses  
390 evoked by exogenous application of 3, 10 and 30  $\mu$ M GABA onto the same outside-out patch

391 (n = 9). We found that the GABA concentration accounting for GABA<sub>A</sub>R activity evoked by  
392 KCl application was close to 3  $\mu$ M (Figure 4 A2). Although the estimated concentration of  
393 non-synaptic release of GABA was relatively low, the exogenous application of 3  $\mu$ M GABA  
394 in the presence of 1  $\mu$ M TTX was sufficient to evoke a  $20.6 \pm 6.1$  mV MN depolarization ( $V_h$   
395 = -60 mV;  $E_{Cl} = -30$  mV; n = 7) (Figures 4B2).

396

397 ***V1<sup>R</sup> exhibit heterogeneous excitability patterns at the onset of SNA.***

398 Spontaneous or evoked RC activity was assessed using whole-cell current-clamp  
399 recordings and the open-book SC preparation (Scain et al., 2010). To determine the identity of  
400 recorded INs, GAD67eGFP neurons were filled with neurobiotin ( $\approx 1$  mg/mL) in combination  
401 with post-hoc Foxd3 staining (Figures 1D). At E12.5, V1<sup>R</sup> had a whole-cell capacitance of  
402  $13.7 \pm 3.8$  pF (n = 192) and an input resistance of  $1242 \pm 620$  M $\Omega$  (n = 192). Spontaneous  
403 activity recorded in 37 V1<sup>R</sup> was characterized by recurrent GDPs (Figure 5), occurring every  
404  $3.7 \pm 2.4$  min (n = 30), similar to what has been observed in MNs ( $\sim 3$  min) (Czarnecki et al.,  
405 2014). Interestingly, in 21.6% (n = 8/37) of the recorded V1<sup>R</sup>, GDPs evoked long-lasting  
406 depolarizing plateau potentials (Figure 5A), while 37.8% (n = 14/37) of the recorded V1<sup>R</sup> had  
407 the ability to spike repetitively during GDPs (Figure 5B). Plateau potentials had an absolute  
408 amplitude of  $53.4 \pm 11.5$  mV (n = 8) and a half amplitude duration ranging from 0.12 to 0.86  
409 s ( $0.44 \pm 0.22$  s; n = 8). In 16.2% (n = 6/37) of the recorded V1<sup>R</sup>, GDPs evoked a single spike  
410 or a doublet (figure 5C), while the remaining 24.3% (n = 9/37) of the recorded V1<sup>R</sup> did not  
411 spike during GDPs (data not shown). These data show that V1<sup>R</sup> can generate various  
412 spontaneous activity patterns and raise the question of their intrinsic activation properties.

413 To analyze the intrinsic activation properties of embryonic V1<sup>R</sup>, we depolarized the  
414 cells from a holding potential of -60 mV using 2 s step current pulses or 20 s depolarizing  
415 current ramps. At E12.5, all V1<sup>R</sup> were excitable (n = 164), but depolarizing current injections  
416 triggered various and complex excitability patterns (Figure 6). 28.7% (n = 47/164) of the

417 analyzed  $V1^R$  were able to generate 1 to 3 action potentials (APs) in response to  
418 suprathreshold depolarizing steps (Figure 6A). When a depolarizing ramp was applied, only  
419 fast membrane potential oscillations of small amplitude were observed. We called these  $V1^R$ ,  
420 SS- $V1^R$ , (“single” spiking  $V1^R$ ). In contrast, 21.2% ( $n = 36/164$ ) of the recorded  $V1^R$  were  
421 able to generate long-lasting events defined as plateau potentials in response to depolarizing  
422 current pulses and in response to depolarizing current ramps. These plateau potentials were  
423 all-or-none events (Figure 6B). They can be evoked by long depolarizing pulses (2s) (Figure  
424 6B) and short depolarizing current pulses (Figure 6F2). They had a half amplitude duration of  
425  $\approx 700$  ms and an absolute peak amplitude of  $\approx 3$  mV (Table 2). Remarkably, these plateau  
426 potentials were sodium-dependent events as they were fully blocked by the application of 1  
427  $\mu$ M TTX (Figure 6F1). Unlike SS- $V1^R$ , these  $V1^R$  can generate repetitive plateau potentials  
428 when depolarized by a suprathreshold depolarizing current ramp (Figure 6B). We called these  
429  $V1^R$ , PP- $V1^R$  (plateau potential  $V1^R$ ). A third group of  $V1^R$  (41.5%;  $n = 68/164$ ) was  
430 identified based on their ability to generate repetitive AP firing in response to suprathreshold  
431 depolarizing current steps or to depolarizing current ramps. In these cells, APs had a half  
432 amplitude duration  $\approx 13$  ms (Table 2). We called these  $V1^R$ , RS- $V1^R$  (repetitive spiking  $V1^R$ )  
433 (Figure 6C). Finally, a fourth group of cells (8.5%;  $n = 14/164$ ) was determined according to  
434 their ability to generate both APs and plateau potential-like events (Figure 6D). We called  
435 these  $V1^R$ , ME- $V1^R$  (mixed event  $V1^R$ ). SS- $V1^R$  are unlikely to be dying neurons.  
436 Developmental cell death (DCD) of V1 INs occurs after E14.5 in mouse embryos (Prasad et  
437 al., 2008) and SS- $V1^R$  passive electrical properties did not differ from those of more active  
438  $V1^R$  (Table 2).

439 Considering that the different types of intrinsic activation pattern may reflect a  
440 continuum between a single spike and a plateau potential, we chose to focus our study on the  
441 three clear patterns of intrinsic activation, SS- $V1^R$ , RS- $V1^R$  and PP- $V1^R$ , and to not study the  
442 mixed regime in depth. Table 2 summarizes passive and active intrinsic electrical properties

443 of recorded SS-V1<sup>R</sup>, RS-V1<sup>R</sup> and PP-V1<sup>R</sup>. Note that the difference in intrinsic excitability in  
444 these different classes of V1<sup>R</sup> is not due to difference in their membrane resistance ( $P > 0.1$ ).

445 These results reveal that V1<sup>R</sup> can have different regimes of activity in the embryonic SC  
446 at the onset of synaptogenesis and SNA (E12.5) (Scain et al., 2010; Czarnecki et al., 2014).

447

448 ***Sustained discharge in embryonic V1<sup>R</sup> depends on persistent sodium current.***

449 A key element in neurons, which exhibit sustained discharges, is the expression of  
450 subthreshold slow-inactivating inward currents. Among these inward currents, the TTX-  
451 sensitive persistent inward current ( $I_{\text{Nap}}$ ) plays a fundamental role in controlling sustained  
452 discharge in INs and MNs in the SC at postnatal developmental stages (Lee and Heckman,  
453 1998; Kuo et al., 2006; Theiss et al., 2007; Ziskind-Conhaim et al., 2008).

454 To determine whether  $I_{\text{Nap}}$  is already expressed by V1<sup>R</sup> in E12.5 mouse embryo, we  
455 made whole-cell voltage-clamp recordings. In this set of experiments, the electrodes were  
456 filled with a Cs-based intracellular solution to minimize contamination of the recorded current  
457 by potassium currents. A test pulse from -100 to -20 mV evoked TTX-sensitive sodium  
458 currents: a large amplitude transient current ( $I_{\text{NaT}}$ ) followed by a smaller amplitude current  
459 persisting over 0.5 s was also fully blocked by TTX (Figure 7A1, inset), which indicates the  
460 presence of  $I_{\text{Nap}}$ . This also indicates that sodium-independent voltage-gated inward currents  
461 were not detected at this developmental stage. To characterize  $I_{\text{Nap}}$  better, we used a slow  
462 voltage ramp (70 mV/s) from -100 to +20 mV designed to inactivate transient currents  
463 (Huang and Trussell, 2008). Subtraction of the trace after TTX application revealed the  $I_{\text{Nap}}$   
464 on the I-V curve (Figure 7A1).  $I_{\text{Nap}}$  was observed in all recorded RCs. We further investigated  
465 the activation properties of the  $I_{\text{Nap}}$ . The Boltzmann fit of the voltage dependence of the  $I_{\text{Nap}}$   
466 generated by voltage ramps revealed a  $V_{\text{half}}$  of  $-22.9 \pm 5.7$  mV and a slope factor ( $k$ ) of  $7.0 \pm$   
467  $1.8$  mV in RCs ( $n = 8$ ) (Figure 7A2). In RCs, the  $I_{\text{Nap}}$  activated at  $V_h = -67.4 \pm 6.2$  mV ( $n = 8$ )

468 and the mean persistent sodium conductance density ( $g_{\text{Nap}}/\text{pF}$ ) was  $41.8 \pm 22.7$  pS/pF ( $n = 12$ )  
469 (Figure 7B).

470 To further confirm that this persistent inward current truly reflects the presence of  $I_{\text{Nap}}$ ,  
471 we tested the effect of a low concentration of riluzole ( $5 \mu\text{M}$ ), which is known to block  $I_{\text{Nap}}$   
472 (Urbani and Belluzzi, 2000). Indeed,  $5 \mu\text{M}$  riluzole suppressed  $81.5 \pm 14.6\%$  ( $n = 15$ ;  $P =$   
473  $0.0005$ ) of the  $I_{\text{Nap}}$  in  $\text{V1}^{\text{R}}$  (Figure 7C), whereas at this low concentration riluzole only slightly  
474 reduced the peak amplitude of  $I_{\text{NaT}}$  (see red arrows in Figure 7A1, inset). We confirmed on  
475 MNs that this low concentration had a minimal effect on the sodium-dependent AP, which  
476 was not the case when riluzole concentration was increased to  $10 \mu\text{M}$  (Figures 8A and 8B1-  
477 B3). AP amplitude was significantly reduced to  $83.2 \pm 12.6\%$  of control in the presence of  $5$   
478  $\mu\text{M}$  riluzole ( $n = 7$ ;  $P = 0.008$ ), but was reduced to  $67.5 \pm 17.0\%$  of control when riluzole  
479 concentration was increased to  $10 \mu\text{M}$  ( $n = 7$ ,  $P = 0.0078$ ). We then reasoned that the lack of  
480 repetitive spiking or plateau potential activity observed in some  $\text{V1}^{\text{R}}$  might depend on a  
481 reduced level of  $I_{\text{Nap}}$ . To test this hypothesis, we compared the presence of  $I_{\text{Nap}}$  in  $\text{V1}^{\text{R}}$  that  
482 cannot generate repetitive spiking (SS- $\text{V1}^{\text{R}}$ ) with  $\text{V1}^{\text{R}}$  that can generate repetitive spiking  
483 (RS- $\text{V1}^{\text{R}}$ ) and with  $\text{V1}^{\text{R}}$  generating plateau potentials (PP- $\text{V1}^{\text{R}}$ ). We developed a voltage- and  
484 current-clamp recording protocol in a given neuron allowing us to associate the amplitude of  
485 the  $I_{\text{Nap}}$  with the excitability pattern in each type of spinal neuron (K-methanesulfonate  
486 intracellular solution) (Figure 9 A1-A4). The same voltage ramp ( $70 \text{ mV/s}$ ) was used as  
487 described above. The  $I_{\text{Nap}}$  current was revealed by subtracting ramp-evoked current in the  
488 presence of  $1 \mu\text{M}$  TTX from controls. In these conditions, SS- $\text{V1}^{\text{R}}$  had a significantly lower  
489  $g_{\text{Nap}}$  density ( $22.1 \pm 12.6$  pS/pF,  $n = 13$ ) when compared to RS- $\text{V1}^{\text{R}}$  ( $57.8 \pm 17.4$  pS/pF,  $n = 7$ )  
490 and to PP- $\text{V1}^{\text{R}}$  ( $70.6 \pm 34.0$  pS/pF,  $n = 11$ ;  $P < 0.0001$ ) (Figure 9A4). These results highlight a  
491 direct relationship between the strength of  $I_{\text{Nap}}$  and the ability of  $\text{V1}^{\text{R}}$  to sustain repetitive  
492 spiking and plateau potential activity.

493 To determine whether  $I_{NaP}$  is required for repetitive spiking in embryonic  $V1^R$ , we  
494 assessed the effect of riluzole on  $V1^R$  that can sustain AP firing or plateau potential activity.  
495 The application of 5  $\mu$ M riluzole turned all RS- $V1^R$  into SS- $V1^R$  ( $n = 10$ ) (Figure 9B). In the  
496 presence of 5  $\mu$ M riluzole, the depolarizing current step failed to trigger more than a doublet  
497 in these cells. 5  $\mu$ M riluzole did not significantly change the AP threshold ( $-37.2 \pm 3.2$  mV vs  
498  $-36.8 \pm 6.0$  mV with 5  $\mu$ M riluzole,  $n = 10$ ,  $P = 0.70$ ). In all PP- $V1^R$ , riluzole prevented the  
499 plateau potential activity ( $n = 7$ ) (Figure 9C). Increasing the amplitude of the injected current  
500 failed to evoke any AP, indicating that PP-RCs were turned into non-excitabile neurons when  
501  $I_{NaP}$  was blocked.

502 Altogether, these results indicate that  $I_{NaP}$  already plays an important role in  $V1^R$   
503 intrinsic activation properties at this early embryonic developmental stage of SC neuronal  
504 networks.

505

506 ***Blocking persistent sodium current alters SNA pattern and SNA propagation along the***  
507 ***cord.***

508 Synchronous activation of MNs and INs was proposed to drive episodes of activity  
509 during SNA (Hanson and Landmesser, 2003; Czarnecki et al., 2014). If intrinsic activation  
510 properties of the few INs that produce GABA including  $V1^R$ , rely on the  $I_{NaP}$ , we expected  
511 that blocking  $I_{NaP}$  would alter episodes of activity during SNA in a manner similar to that  
512 observed in the presence of GABA<sub>A</sub>R antagonists (Hanson and Landmesser, 2003; Czarnecki  
513 et al., 2014). Blocking GABA neurotransmission during SNA evoked an increase in inter-  
514 episode interval, but had little effect on the duration of episode of activity and on their  
515 propagation along the cord (Hanson and Landmesser, 2003). In addition, we previously  
516 showed that blocking GABA neurotransmission decreased the amplitude of spontaneous giant  
517 inward currents (sGICs) recorded in MNs during SNA (Czarnecki et al., 2014).

518 To determine the involvement of  $I_{NaP}$  in SNA, we first tested the effect of 5  $\mu$ M riluzole

519 on the spontaneous activity of MNs using whole-cell voltage-clamp recordings. In control  
520 conditions, sGICs occurred every 4 minutes ( $4.0 \pm 0.8$  min,  $n = 9$ ), had mean amplitude of  
521  $291 \pm 200$  pA ( $n = 9$ ) and a half-width of  $0.6 \pm 0.3$  s ( $V_h = -60$  mV;  $E_{Cl} = 3$  mV) (Figure  
522 10A1-A2). The time course of the effect of riluzole on sGIC occurrence was variable among  
523 MNs. In one out of nine recorded MNs, riluzole abolished GIC activity in less than 10 min. In  
524 other MNs, 1 to 2 GICs could still be observed during the 20- to 30-min application of  
525 riluzole. (Figure 10A2). During this transitory period, riluzole significantly reduced the  
526 amplitude of GICs ( $30.8 \pm 32.7\%$  reduction;  $n = 8$ ;  $P = 0.039$ ) (Figure 10B1) and the half-  
527 duration of GICs ( $44.0 \pm 27.2\%$  reduction;  $n = 8$ ;  $P = 0.0078$ ) (Figure 10B2). In order to assess  
528 the effect of riluzole on SNA, we made long-lasting extracellular recordings of SC activity  
529 using two electrodes positioned on the cervical and lumbar superficial part of the ventral horn  
530 of the SC at E12.5 (Czarnecki et al., 2014) (Figure 10C1).

531 These recordings allowed us to monitor SC neuron activity related to GIC activity  
532 recorded in MNs (Czarnecki et al., 2014). We found that a 30- to 40-min application of  $5 \mu\text{M}$   
533 riluzole significantly increased the inter-episode interval from  $4.18 \pm 1.93$  min in control  
534 conditions to  $12.34 \pm 9.08$  min in the presence of riluzole ( $P < 0.001$ ,  $n = 12$  paired SCs)  
535 ( $196.3 \pm 203\%$  increase) (Figure 10C2-C3), revealing a strong involvement of the  $I_{\text{Nap}}$  current  
536 in the rhythmicity of early SC network activity. We therefore analyzed individual bursts of  
537 AP exhibited by the cervical (C) and lumbar (L) SC networks in the presence of riluzole. We  
538 found that the duration of bursts (both C and L), compared before ( $2.31 \pm 0.89$  s) and after the  
539 riluzole application ( $1.44 \pm 0.7$  s), was significantly reduced ( $36.5 \pm 18.3\%$  reduction;  $n = 22$ ;  
540  $P < 0.001$ ) (Figure 10C4). In addition, the instantaneous AP frequency within a burst at both  
541 the cervical level (C level) and the lumbar level (L level) was significantly reduced by  $25.3 \pm$   
542  $11.9\%$  ( $P < 0.001$ ) in the presence of riluzole ( $112.4 \pm 39.6$  Hz in control conditions and  $83.3$   
543  $\pm 34.4$  Hz with riluzole,  $n = 22$ ) (Figure 10C5). We also observed a reduction in the speed of  
544 propagation of SNA episodes between the C level and L level of the SC in the presence of



545 riluzole. Propagation of SNA along the cord was investigated by analysis of the time needed  
546 for a burst of AP recorded at the C level to reach L level (distance between the two recording  
547 levels  $\approx$  4mm) (Yvert et al., 2004). We found that the C-L time was significantly increased ( $P$   
548  $< 0.001$ ) from  $1.56 \pm 0.42$  s in control conditions to  $2.42 \pm 0.77$  s in the presence of riluzole  
549 ( $56.3 \pm 36.1\%$  increase;  $n = 10$ ) (Figure 10C6).

550 Riluzole had a stronger effect on SNA than previously observed in the presence of  
551 GABA<sub>A</sub>R antagonists (Hanson and Landmesser, 2003; Czarnecki et al., 2014). Targeted  
552 networks during extracellular recordings likely include MNs as well as surrounding INs  
553 (Hanson and Landmesser, 2003; Czarnecki et al., 2014) including V1<sup>R</sup> GABAergic INs.  
554 Because most GABAergic V1<sup>R</sup> are able to generate repetitive firing in response to GDP,  
555 which is not the case for MNs (Czarnecki et al., 2014), this apparent discrepancy could be  
556 explained if blocking GABA neurotransmission does not strongly alter GABAergic INs  
557 firing, just as riluzole does. We cannot, however, exclude that  $I_{\text{Nap}}$  is also present in neurons  
558 other than V1<sup>R</sup> in the SC at E12.5. Anyhow, these results indicate that  $I_{\text{Nap}}$  plays an important  
559 role in SNA at the onset of synaptogenesis (E12.5) by regulating neuron excitability in the  
560 mouse embryonic SC.

561 **DISCUSSION**

562       How excitability of neurons evolves during SC development was extensively studied at  
563 developmental stages at which central pattern generators are already functional. At these  
564 developmental stages (P0 to P5, postnatal day),  $I_{\text{Nap}}$  is present in MNs and in SC INs (Tazerart  
565 et al., 2007; Zhong et al., 2007) and is required to generate fictive locomotion (Zhong et al.,  
566 2007). Here, we show that  $V1^{\text{R}}$  already express  $I_{\text{Nap}}$  at the onset of synaptogenesis in the  
567 embryonic (E12.5) SC (Scain et al., 2010). Our results reveal that  $I_{\text{Nap}}$  already closely controls  
568 the  $V1^{\text{R}}$  excitability pattern. In addition, we found that low concentrations of riluzole, an  $I_{\text{Nap}}$   
569 blocker, dramatically altered the SC SNA pattern, suggesting that  $I_{\text{Nap}}$  is already expressed by  
570 neurons in the mammalian embryonic SC well before the control of muscle contraction by  
571 MNs (Sanes and Lichtman, 1999).

572

573  ***$V1^{\text{R}}$  display different excitability patterns at the onset of SNA.***

574       Repetitive firing of presynaptic neurons is required for long-lasting neurotransmitter-  
575 dependent episodes, as GDPs observed in MNs at E12.5. Previous studies have examined the  
576 development of passive and active membrane properties of MNs and INs in late embryonic  
577 and newborn rats or mice (Ziskind-Conhaim, 1988; Gao and Ziskind-Conhaim, 1998; Vinay  
578 et al., 2000; Theiss et al., 2007; Perry et al., 2015; Bikoff et al., 2016), but there is no  
579 information about the excitability of INs at early mammalian embryonic developmental stages  
580 when SNA first arises. We found that a majority of  $V1^{\text{R}}$  ( $\approx 60\%$ ) can already generate  
581 repetitive AP firing or long-lasting sodium-dependent plateau potentials at the onset of SNA,  
582 indicating that these cells are already active at this early embryonic developmental stage. Our  
583 analysis revealed a strong heterogeneity in  $V1^{\text{R}}$  excitability pattern, which can be separated  
584 into different independent classes, but such functional diversity is unlikely to persist in the  
585 adult. In the adult,  $V1^{\text{R}}$  were found to generate two different excitability patterns only, a  
586 prominent low-threshold depolarization and burst firing followed by continuous firing

587 dependent on  $V_h$  (Perry et al., 2015; Bikoff et al., 2016). It is therefore likely that the  
588 functional heterogeneity we observed at E12.5 reflects an immature form of  $V1^R$  excitability  
589 (Perry et al., 2015; Bikoff et al., 2016). Sodium-dependent plateau potentials were also  
590 observed in ipsilateral caudal SC INs of zebrafish embryos at the appearance of functional  
591 neuromuscular junctions and then disappeared at more mature stages (Tong and McDermid,  
592 2012).

593

594  ***$I_{Nap}$  already regulate excitability patterns of  $V1^R$  at early developmental stages.***

595 In this study, we reveal the presence of  $I_{Nap}$  in neurons of mammalian embryos at the  
596 onset of SNA. Persistent inward currents (PICs) are present in many types of neurons. PICs  
597 can be calcium- and/or sodium-dependent depending on the neuron subtypes. We did not find  
598 any evidence for a significant calcium component in recorded PICs in  $V1^R$  at E12.5. Indeed,  
599 the PIC was fully blocked by TTX in  $V1^R$ , which contrasts with what is known about more  
600 mature spinal neurons like MNs (Hounsgaard and Kiehn, 1989; Bui et al., 2006; Carlin et al.,  
601 2009). Accordingly, we concluded that immature  $V1^R$  at the onset of SNA generate a pure  
602 sodium-dependent PIC.  $I_{Nap}$  recorded in  $V1^R$  of the mouse embryo has an activation onset ( $\approx$  -  
603 65 mV) similar to that of  $I_{Nap}$  at postnatal developmental stages in the rat and mouse SC (Kuo  
604 et al., 2006; Tazerart et al., 2007; Theiss et al., 2007; Tazerart et al., 2008; Dai and Jordan,  
605 2010). The Boltzmann constant of activation calculated for  $I_{Nap}$  in  $V1^R$  ( $\approx$  7 mV) is in the  
606 range of the values known for  $I_{Nap}$  in INs and MNs ( $\approx$  6 mV) of neonatal rats (Bouhadfane et  
607 al., 2013) or in the calyx of Held ( $\approx$  8 mV) (Huang and Trussell, 2008). Small differences in  
608 the voltage dependency of  $I_{Nap}$  activation may reflect differences in sodium channel  $\alpha$ -subunit  
609 and/or  $\beta$ -subunit combination expression (Isom et al., 1994; Qu et al., 2001).

610  $I_{Nap}$  likely has diverse functions and plays an important function in locomotor pattern  
611 generation in neonatal rats (Tazerart, S., *et al.* 2007). In neonate SC,  $I_{Nap}$  is present in both  
612 INs and MNs (Kuo et al., 2006; Tazerart et al., 2007) and is known to generate pacemaker

613 activities in central pattern generator INs (Tazerart et al., 2008). Remarkably,  $I_{Nap}$  also  
614 contributes to lumbar MN activity related to plateau potential in rat neonates (Bouhadfane et  
615 al., 2013). However, while in neonate MNs,  $I_{Nap}$  is essential for self-sustained firing only  
616 during calcium-dependent plateau potential depolarization (Carlin et al., 2009; Bouhadfane et  
617 al., 2013), plateau potential activity in  $V1^R$  at E12.5 is fully  $I_{Nap}$ -dependent

618

619 ***Does  $I_{Nap}$  already participate in SC activity at the onset of neuronal network formation?***

620  $I_{Nap}$  plays a crucial role in the regulation of locomotor pattern generation in rat  
621 neonates (Tazerart et al., 2007; Zhong et al., 2007; Bouhadfane et al., 2013) and in the SC of  
622 the zebrafish embryo during the cooling stage (Tong and McDearmid, 2012). Here, we  
623 demonstrated that a low concentration of riluzole dramatically reduced the amplitude and the  
624 duration of GICs recorded on MNs and strongly altered SC activity (extracellular recordings)  
625 at the onset of SNA.

626 In our experiments, we used a concentration of riluzole that has a minimal effect on the  
627 sodium AP waveform (Figure 6). However, beside its effect on  $I_{Nap}$ , riluzole is known to  
628 inhibit the release of glutamate (Cheramy et al., 1992), to inhibit AMPA receptor activation  
629 (Albo et al., 2004), GABA<sub>A</sub> and glycine receptor activation (Mohammadi et al., 2001) and to  
630 block several voltage-gated channels including calcium channels (Huang et al., 1997; Ahn et  
631 al., 2006). With the exception of AMPA receptor inhibition (Albo et al., 2004), these side  
632 effects of riluzole occur at concentrations  $\geq 10 \mu\text{M}$  (Cheramy et al., 1992; Huang et al., 1997;  
633 Mohammadi et al., 2001; Ahn et al., 2006). Because the inhibition of glutamate  
634 neurotransmission did not alter SNA in the mouse embryonic SC at E12.5 (Czarnecki et al.,  
635 2014), it is unlikely that the alteration of SNA we observed in the presence of  $5 \mu\text{M}$  riluzole is  
636 caused by the inhibition of glutamatergic synaptic activity (Albo et al., 2004). Accordingly,  
637 we propose that  $I_{Nap}$  already regulates the SNA pattern at the onset of synaptogenesis in  
638 mammalian embryos before the formation of the locomotor SC network and of functional

639 neuromuscular junctions. However, we cannot exclude that spinal neurons other than  $V1^R$   
640 exhibit  $I_{Nap}$ -dependent sustain discharge at this developmental stage.

641 Because  $V1^R$  already produce GABA at E12.5 and make synaptic-like contacts with  
642 MNs while MNs make synaptic-like contacts with  $V1^R$  (see also (Alvarez et al., 2013), it is  
643 likely that  $V1^R$  participate in early SC SNA. Although correlative, our data reinforce the  
644 hypothesis that a primitive  $V1^R$ -MN recurrent-like circuit may exist at the onset of  
645 synaptogenesis in the mouse embryo. This primitive  $V1^R$ -MN recurrent circuit differs in  
646 several ways from the adult RC-MN recurrent circuits. Evoked MN spiking did not trigger a  
647 recurrent synaptic response at E12.5 (Le Bras et al., 2014), which suggests that although  $V1^R$   
648 projects on MNs and vice versa, it is unlikely that  $V1^R$  projecting on MNs receive inputs from  
649 these MNs and vice versa. It is also unlikely that MN release sites apposed on  $V1^R$  are mixed  
650 glutamatergic and cholinergic inputs as observed at postnatal stages (Nishimaru et al., 2005;  
651 Lamotte d'Incamps et al., 2017). Glutamatergic vesicular transporters were not observed  
652 within MNs at E12.5 (Czarnecki et al., 2014). But we cannot completely exclude that some  
653 immature motor axon synapses on  $V1^R$  already release aspartate, as suggested in the adult  
654 (Richards et al., 2014). However, contrary to what is observed for GABAergic and  
655 cholinergic networks, the spontaneous activation of glutamate receptors had a minor role only  
656 in the generation of SNA episodes at E12.5 (Czarnecki et al., 2014).

657 We clearly show that paracrine release of GABA can occur in the embryonic SC, which  
658 may explain the smooth shape of GABAergic-dependent GDPs observed in MNs during SNA  
659 (Czarnecki et al., 2014). Since  $V1^R$  are GABAergic at this embryonic age and possess  
660 putative release sites,  $V1^R$  may be one of the sources for the paracrine release of GABA we  
661 observed. Accordingly, we propose that  $V1^R$ -MN interactions occur through synaptic and  
662 paracrine release and participate in the synchronization of neuronal assembly required for the  
663 generation of the propagating waves of activity characterizing SC SNA at E12.5 (Momose-  
664 Sato and Sato, 2013).

665

666 ***Conclusions***

667 Taken together, our findings demonstrate that  $I_{Nap}$  is already present in developing SC  
668 neurons at an early developmental stage and governs  $V1^R$  excitability.  $I_{Nap}$  plays an important  
669 role in the regulation of locomotor pattern generation at postnatal developmental stages in  
670 rodents (Tazerart et al., 2008). Because the application of a low concentration of riluzole  
671 altered SNA, we propose that  $I_{Nap}$  contributes to the patterning of embryonic SC activity at the  
672 onset of synaptogenesis. Accordingly, the capacity of SC neurons to generate sustained firing  
673 must be crucial for correct embryonic SC patterned activity at the onset of synaptogenesis,  
674 which is required for the correct development of MN projections toward their peripheral  
675 targets (Hanson and Landmesser, 2006).

676

677 **BIBLIOGRAPHY**

- 678 Ahn HS, Kim SE, Jang HJ, Kim MJ, Rhie DJ, Yoon SH, Jo YH, Kim MS, Sung KW, Hahn  
679 SJ (2006) Interaction of riluzole with the closed inactivated state of Kv4.3 channels.  
680 *The Journal of pharmacology and experimental therapeutics* 319:323-331.
- 681 Albo F, Pieri M, Zona C (2004) Modulation of AMPA receptors in spinal motor neurons by  
682 the neuroprotective agent riluzole. *Journal of neuroscience research* 78:200-207.
- 683 Allain AE, Bairi A, Meyrand P, Branchereau P (2004) Ontogenic changes of the GABAergic  
684 system in the embryonic mouse spinal cord. *Brain research* 1000:134-147.
- 685 Allain AE, Bairi A, Meyrand P, Branchereau P (2006) Expression of the glycinergic system  
686 during the course of embryonic development in the mouse spinal cord and its co-  
687 localization with GABA immunoreactivity. *The Journal of comparative neurology*  
688 496:832-846.
- 689 Alvarez FJ, Benito-Gonzalez A, Siembab VC (2013) Principles of interneuron development  
690 learned from Renshaw cells and the motoneuron recurrent inhibitory circuit. *Annals of*  
691 *the New York Academy of Sciences* 1279:22-31.
- 692 Barberis A, Mozrzymas JW, Ortinski PI, Vicini S (2007) Desensitization and binding  
693 properties determine distinct  $\alpha 1\beta 2\gamma 2$  and  $\alpha 3\beta 2\gamma 2$  GABA(A)  
694 receptor-channel kinetic behavior. *The European journal of neuroscience* 25:2726-  
695 2740.
- 696 Ben-Ari Y, Cherubini E, Corradetti R, Gaiarsa JL (1989) Giant synaptic potentials in  
697 immature rat CA3 hippocampal neurones. *J Physiol* 416:303-325.
- 698 Benito-Gonzalez A, Alvarez FJ (2012) Renshaw cells and Ia inhibitory interneurons are  
699 generated at different times from p1 progenitors and differentiate shortly after exiting  
700 the cell cycle. *J Neurosci* 32:1156-1170.
- 701 Bikoff JB, Gabitto MI, Rivard AF, Drobac E, Machado TA, Miri A, Brenner-Morton S,  
702 Famojure E, Diaz C, Alvarez FJ, Mentis GZ, Jessell TM (2016) Spinal Inhibitory  
703 Interneuron Diversity Delineates Variant Motor Microcircuits. *Cell* 165:207-219.
- 704 Bouhadfane M, Tazerart S, Moqrish A, Vinay L, Brocard F (2013) Sodium-mediated plateau  
705 potentials in lumbar motoneurons of neonatal rats. *J Neurosci* 33:15626-15641.
- 706 Bui TV, Ter-Mikaelian M, Bedrossian D, Rose PK (2006) Computational estimation of the  
707 distribution of L-type  $\text{Ca}^{2+}$  channels in motoneurons based on variable threshold of  
708 activation of persistent inward currents. *Journal of neurophysiology* 95:225-241.
- 709 Carlin KP, Bui TV, Dai Y, Brownstone RM (2009) Staircase currents in motoneurons: insight  
710 into the spatial arrangement of calcium channels in the dendritic tree. *J Neurosci*  
711 29:5343-5353.
- 712 Carr PA, Alvarez FJ, Leman EA, Fyffe RE (1998) Calbindin D28k expression in  
713 immunohistochemically identified Renshaw cells. *Neuroreport* 9:2657-2661.
- 714 Cheramy A, Barbeito L, Godeheu G, Glowinski J (1992) Riluzole inhibits the release of  
715 glutamate in the caudate nucleus of the cat in vivo. *Neuroscience letters* 147:209-212.
- 716 Corlew R, Bosma MM, Moody WJ (2004) Spontaneous, synchronous electrical activity in  
717 neonatal mouse cortical neurones. *J Physiol* 560:377-390.
- 718 Czarnecki A, Le Corrionc H, Rigato C, Le Bras B, Couraud F, Scain AL, Allain AE, Mouffle  
719 C, Bullier E, Mangin JM, Branchereau P, Legendre P (2014) Acetylcholine controls  
720 GABA-, glutamate-, and glycine-dependent giant depolarizing potentials that govern  
721 spontaneous motoneuron activity at the onset of synaptogenesis in the mouse  
722 embryonic spinal cord. *J Neurosci* 34:6389-6404.
- 723 Dai Y, Jordan LM (2010) Multiple patterns and components of persistent inward current with  
724 serotonergic modulation in locomotor activity-related neurons in Cfos-EGFP mice.  
725 *Journal of neurophysiology* 103:1712-1727.

- 726 Delpy A, Allain AE, Meyrand P, Branchereau P (2008) NKCC1 cotransporter inactivation  
727 underlies embryonic development of chloride-mediated inhibition in mouse spinal  
728 motoneuron. *J Physiol* 586:1059-1075.
- 729 Dottori M, Gross MK, Labosky P, Goulding M (2001) The winged-helix transcription factor  
730 *Foxd3* suppresses interneuron differentiation and promotes neural crest cell fate.  
731 *Development* 128:4127-4138.
- 732 Eccles JC, Fatt P, Landgren S (1956) The inhibitory pathway to motoneurons. *Progress in*  
733 *neurobiology*:72-82.
- 734 Feller MB (1999) Spontaneous correlated activity in developing neural circuits. *Neuron*  
735 22:653-656.
- 736 Gao BX, Ziskind-Conhaim L (1998) Development of ionic currents underlying changes in  
737 action potential waveforms in rat spinal motoneurons. *Journal of neurophysiology*  
738 80:3047-3061.
- 739 Garaschuk O, Hanse E, Konnerth A (1998) Developmental profile and synaptic origin of  
740 early network oscillations in the CA1 region of rat neonatal hippocampus. *J Physiol*  
741 507 ( Pt 1):219-236.
- 742 Garaschuk O, Linn J, Eilers J, Konnerth A (2000) Large-scale oscillatory calcium waves in  
743 the immature cortex. *Nat Neurosci* 3:452-459.
- 744 Geiman EJ, Knox MC, Alvarez FJ (2000) Postnatal maturation of gephyrin/glycine receptor  
745 clusters on developing Renshaw cells. *The Journal of comparative neurology* 426:130-  
746 142.
- 747 Gonzalez-Islas C, Wenner P (2006) Spontaneous network activity in the embryonic spinal  
748 cord regulates AMPAergic and GABAergic synaptic strength. *Neuron* 49:563-575.
- 749 Gust J, Wright JJ, Pratt EB, Bosma MM (2003) Development of synchronized activity of  
750 cranial motor neurons in the segmented embryonic mouse hindbrain. *J Physiol*  
751 550:123-133.
- 752 Hanson MG, Landmesser LT (2003) Characterization of the circuits that generate  
753 spontaneous episodes of activity in the early embryonic mouse spinal cord. *J Neurosci*  
754 23:587-600.
- 755 Hanson MG, Landmesser LT (2006) Increasing the frequency of spontaneous rhythmic  
756 activity disrupts pool-specific axon fasciculation and pathfinding of embryonic spinal  
757 motoneurons. *J Neurosci* 26:12769-12780.
- 758 Hanson MG, Milner LD, Landmesser LT (2008) Spontaneous rhythmic activity in early chick  
759 spinal cord influences distinct motor axon pathfinding decisions. *Brain Res Rev*  
760 57:77-85.
- 761 Hounsgaard J, Kiehn O (1989) Serotonin-induced bistability of turtle motoneurons caused by  
762 a nifedipine-sensitive calcium plateau potential. *J Physiol* 414:265-282.
- 763 Huang CS, Song JH, Nagata K, Yeh JZ, Narahashi T (1997) Effects of the neuroprotective  
764 agent riluzole on the high voltage-activated calcium channels of rat dorsal root  
765 ganglion neurons. *The Journal of pharmacology and experimental therapeutics*  
766 282:1280-1290.
- 767 Huang H, Trussell LO (2008) Control of presynaptic function by a persistent Na(+) current.  
768 *Neuron* 60:975-979.
- 769 Isom LL, De Jongh KS, Catterall WA (1994) Auxiliary subunits of voltage-gated ion  
770 channels. *Neuron* 12:1183-1194.
- 771 Kirkby LA, Sack GS, Firl A, Feller MB (2013) A role for correlated spontaneous activity in  
772 the assembly of neural circuits. *Neuron* 80:1129-1144.
- 773 Kuo JJ, Lee RH, Zhang L, Heckman CJ (2006) Essential role of the persistent sodium current  
774 in spike initiation during slowly rising inputs in mouse spinal neurones. *J Physiol*  
775 574:819-834.



- 776 Lamotte d'Incamps B, Bhumbra GS, Foster JD, Beato M, Ascher P (2017) Segregation of  
777 glutamatergic and cholinergic transmission at the mixed motoneuron Renshaw cell  
778 synapse. *Scientific reports* 7:4037.
- 779 Landmesser LT, O'Donovan MJ (1984) Activation patterns of embryonic chick hind limb  
780 muscles recorded in ovo and in an isolated spinal cord preparation. *J Physiol* 347:189-  
781 204.
- 782 Le Bras B, Freal A, Czarnecki A, Legendre P, Bullier E, Komada M, Brophy PJ, Davenne M,  
783 Couraud F (2014) In vivo assembly of the axon initial segment in motor neurons.  
784 *Brain structure & function* 219:1433-1450.
- 785 Le-Corronc H, Rigo JM, Branchereau P, Legendre P (2011) GABA(A) receptor and glycine  
786 receptor activation by paracrine/autocrine release of endogenous agonists: more than a  
787 simple communication pathway. *Molecular neurobiology* 44:28-52.
- 788 Lee RH, Heckman CJ (1998) Bistability in spinal motoneurons in vivo: systematic variations  
789 in persistent inward currents. *Journal of neurophysiology* 80:583-593.
- 790 Marder E, Rehm KJ (2005) Development of central pattern generating circuits. *Curr Opin*  
791 *Neurobiol* 15:86-93.
- 792 Mohammadi B, Krampfl K, Moschref H, Dengler R, Bufler J (2001) Interaction of the  
793 neuroprotective drug riluzole with GABA(A) and glycine receptor channels. *European*  
794 *journal of pharmacology* 415:135-140.
- 795 Momose-Sato Y, Sato K (2013) Optical imaging of the spontaneous depolarization wave in  
796 the mouse embryo: origins and pharmacological nature. *Annals of the New York*  
797 *Academy of Sciences* 1279:60-70.
- 798 Moody WJ (1998) Control of spontaneous activity during development. *Journal of*  
799 *neurobiology* 37:97-109.
- 800 Muller A, Kukley M, Stausberg P, Beck H, Muller W, Dietrich D (2005) Endogenous Ca<sup>2+</sup>  
801 buffer concentration and Ca<sup>2+</sup> microdomains in hippocampal neurons. *J Neurosci*  
802 25:558-565.
- 803 Myers CP, Lewcock JW, Hanson MG, Gosgnach S, Aimone JB, Gage FH, Lee KF,  
804 Landmesser LT, Pfaff SL (2005) Cholinergic input is required during embryonic  
805 development to mediate proper assembly of spinal locomotor circuits. *Neuron* 46:37-  
806 49.
- 807 Nishimaru H, Restrepo CE, Ryge J, Yanagawa Y, Kiehn O (2005) Mammalian motor neurons  
808 corelease glutamate and acetylcholine at central synapses. *Proceedings of the National*  
809 *Academy of Sciences of the United States of America* 102:5245-5249.
- 810 Perry S, Gezelius H, Larhammar M, Hilscher MM, Lamotte d'Incamps B, Leao KE,  
811 Kullander K (2015) Firing properties of Renshaw cells defined by *Chrna2* are  
812 modulated by hyperpolarizing and small conductance ion currents *I<sub>h</sub>* and *ISK*. *The*  
813 *European journal of neuroscience* 41:889-900.
- 814 Prasad T, Wang X, Gray PA, Weiner JA (2008) A differential developmental pattern of spinal  
815 interneuron apoptosis during synaptogenesis: insights from genetic analyses of the  
816 *protocadherin-gamma* gene cluster. *Development* 135:4153-4164.
- 817 Qu Y, Curtis R, Lawson D, Gilbride K, Ge P, DiStefano PS, Silos-Santiago I, Catterall WA,  
818 Scheuer T (2001) Differential modulation of sodium channel gating and persistent  
819 sodium currents by the beta1, beta2, and beta3 subunits. *Molecular and cellular*  
820 *neurosciences* 18:570-580.
- 821 Richards DS, Griffith RW, Romer SH, Alvarez FJ (2014) Motor axon synapses on rensaw  
822 cells contain higher levels of aspartate than glutamate. *PloS one* 9:e97240.
- 823 Rockhill W, Kirkman JL, Bosma MM (2009) Spontaneous activity in the developing mouse  
824 midbrain driven by an external pacemaker. *Dev Neurobiol* 69:689-704.
- 825 Safiulina VF, Cherubini E (2009) At immature mossy fibers-CA3 connections, activation of  
826 presynaptic GABA(B) receptors by endogenously released GABA contributes to  
827 synapses silencing. *Frontiers in cellular neuroscience* 3:1.

- 828 Sanes JR, Lichtman JW (1999) Development of the vertebrate neuromuscular junction.  
829 Annual review of neuroscience 22:389-442.
- 830 Sapir T, Geiman EJ, Wang Z, Velasquez T, Mitsui S, Yoshihara Y, Frank E, Alvarez FJ,  
831 Goulding M (2004) Pax6 and engrailed 1 regulate two distinct aspects of rensaw cell  
832 development. *J Neurosci* 24:1255-1264.
- 833 Scain AL, Le Corrone H, Allain AE, Muller E, Rigo JM, Meyrand P, Branchereau P,  
834 Legendre P (2010) Glycine release from radial cells modulates the spontaneous  
835 activity and its propagation during early spinal cord development. *J Neurosci* 30:390-  
836 403.
- 837 Stam FJ, Hendricks TJ, Zhang J, Geiman EJ, Francius C, Labosky PA, Clotman F, Goulding  
838 M (2012) Renshaw cell interneuron specialization is controlled by a temporally  
839 restricted transcription factor program. *Development* 139:179-190.
- 840 Tamamaki N, Yanagawa Y, Tomioka R, Miyazaki J, Obata K, Kaneko T (2003) Green  
841 fluorescent protein expression and colocalization with calretinin, parvalbumin, and  
842 somatostatin in the GAD67-GFP knock-in mouse. *The Journal of comparative*  
843 *neurology* 467:60-79.
- 844 Tazerart S, Vinay L, Brocard F (2008) The persistent sodium current generates pacemaker  
845 activities in the central pattern generator for locomotion and regulates the locomotor  
846 rhythm. *J Neurosci* 28:8577-8589.
- 847 Tazerart S, Viemari JC, Darbon P, Vinay L, Brocard F (2007) Contribution of persistent  
848 sodium current to locomotor pattern generation in neonatal rats. *Journal of*  
849 *neurophysiology* 98:613-628.
- 850 Theiss RD, Kuo JJ, Heckman CJ (2007) Persistent inward currents in rat ventral horn  
851 neurones. *J Physiol* 580:507-522.
- 852 Tong H, McDearmid JR (2012) Pacemaker and plateau potentials shape output of a  
853 developing locomotor network. *Current biology : CB* 22:2285-2293.
- 854 Urbani A, Belluzzi O (2000) Riluzole inhibits the persistent sodium current in mammalian  
855 CNS neurons. *The European journal of neuroscience* 12:3567-3574.
- 856 Vinay L, Brocard F, Pflieger JF, Simeoni-Alias J, Clarac F (2000) Perinatal development of  
857 lumbar motoneurons and their inputs in the rat. *Brain research bulletin* 53:635-647.
- 858 Watt AJ, Cuntz H, Mori M, Nusser Z, Sjöstrom PJ, Häusser M (2009) Traveling waves in  
859 developing cerebellar cortex mediated by asymmetrical Purkinje cell connectivity. *Nat*  
860 *Neurosci* 12:463-473.
- 861 Wenner P, O'Donovan MJ (2001) Mechanisms that initiate spontaneous network activity in  
862 the developing chick spinal cord. *Journal of neurophysiology* 86:1481-1498.
- 863 Wichterle H, Lieberam I, Porter JA, Jessell TM (2002) Directed differentiation of embryonic  
864 stem cells into motor neurons. *Cell* 110:385-397.
- 865 Young SH, Poo MM (1983) Spontaneous release of transmitter from growth cones of  
866 embryonic neurones. *Nature* 305:634-637.
- 867 Yvert B, Branchereau P, Meyrand P (2004) Multiple spontaneous rhythmic activity patterns  
868 generated by the embryonic mouse spinal cord occur within a specific developmental  
869 time window. *Journal of neurophysiology* 91:2101-2109.
- 870 Zhang LI, Poo MM (2001) Electrical activity and development of neural circuits. *Nat*  
871 *Neurosci* 4 Suppl:1207-1214.
- 872 Zhong G, Masino MA, Harris-Warrick RM (2007) Persistent sodium currents participate in  
873 fictive locomotion generation in neonatal mouse spinal cord. *J Neurosci* 27:4507-  
874 4518.
- 875 Ziskind-Conhaim L (1988) Electrical properties of motoneurons in the spinal cord of rat  
876 embryos. *Developmental biology* 128:21-29.
- 877 Ziskind-Conhaim L, Wu L, Wiesner EP (2008) Persistent sodium current contributes to  
878 induced voltage oscillations in locomotor-related hb9 interneurons in the mouse spinal  
879 cord. *Journal of neurophysiology* 100:2254-2264.

880

881 **LEGENDS**882 ***Figure 1: VI<sup>R</sup> identification in the lumbar spinal cord of E12.5 embryos***

883 A) Coronal slice of the lumbar spinal cord of E12.5 GA67-eGFP mouse embryo showing the  
884 distribution of eGFP neurons (A1), FoxD3 (A2) and calbindin (A3) immunoreactive neurons.

885 A4) Superimposed images showing the colocalization of eGFP, FoxD3 immunostaining and  
886 calbindin immunostaining. B) Enlarged images from A showing that eGFP neurons localized  
887 in the ventrolateral area of the spinal cord (B1) are Foxd3 immunoreactive (B2), most of them  
888 being calbindin immunoreactive (B3-B4). C) Coronal slice of the ventrolateral part of the

889 lumbar spinal cord of E12.5 GA67-eGFP mouse embryo showing the distribution of eGFP  
890 neurons (C1), FoxD3 (C2) and MafB (C3) immunoreactive neurons. C4) Superimposed

891 images showing the colocalization of eGFP FoxD3 immunostaining and MafB  
892 immunostaining. Note that all FoxD3 immunoreactive neurons localized in the marginal zone  
893 of the ventrolateral area are also MafB-positive, indicating that they are VI<sup>R</sup> neurons. D1)

894 Example of a neuron filled with neurobiotin during the recording at the lumbar level of an  
895 embryonic spinal cord open book preparation of GAD67-GFP mice at E12.5. This eGFP  
896 neuron (D2) was immunoreactive to Foxd3 antibody (D3), as shown in the merged images  
897 (D4). Each image corresponds to a single confocal section.

898

899 ***Figure 2: VI<sup>R</sup> already produce GABA in the lumbar spinal cord of E12.5 embryos***

900 A) Single confocal sections of coronal slice of the lumbar spinal cord of E12.5 GA67-eGFP  
901 mouse embryo showing the distribution of eGFP neurons (A1), calbindin (A2) and GABA

902 (A3) immunoreactive neurons. A4) Superimposed images showing the colocalization of  
903 eGFP, calbindin immunostaining and GABA immunostaining. B1-B3) Enlarged images from

904 A1, A2 and A3 showing eGFP neurons (B1), calbindin immunoreactive neurons (B2), and  
905 GABA immunoreactive neurons (B3) in the ventrolateral area of the spinal cord. B4)

906 Superimposed images showing the colocalization of calbindin immunostaining and GABA

907 immunostaining with z projections within a stack. Note the colocalization of calbindin  
908 immunostaining and GABA immunostaining in the three axes, indicating that  $V1^R$  already  
909 produce GABA at E12.5.

910

911 ***Figure 3:  $V1^R$  make synaptic-like contacts with motoneurons (HB9-eGFP) at E12.5.***

912 A) Coronal slice of the lumbar spinal cord of E12.5 HB9-eGFP mouse embryo with cell  
913 nucleus staining (Hoesch) and synaptophysin immunostaining (A1). A1) Note that  
914 synaptophysin immunostaining is mainly restricted in the ventral funiculus (VF) A2)  
915 Calbindin staining showing the distribution of  $V1^R$  neurite extensions and synaptophysin  
916 immunostaining. A3) eGFP immunostaining showing the distribution of MN neurite  
917 extensions and synaptophysin immunostaining. Antibody against GFP was used to visualize  
918 MN morphology better (Czarnecki et al., 2014). A4) Superimposition of eGFP fluorescence,  
919 calbindin immunostaining and synaptophysin immunostaining (A1, A2, A3, and A4 are  
920 confocal stacks). B) Single confocal sections with z projections of enlarged images from A2,  
921 A3 and A4 showing the colocalization of synaptophysin punctates with calbindin  
922 immunostaining apposed to eGFP immunostaining (B1, B2 and B3; enlarged images in  
923 boxes). B2) Note that a synaptophysin punctate colocalized with calbindin immunostaining  
924 (B1, arrow) did not colocalize with eGFP immunostaining (B2, arrow). Note that  
925 synaptophysin punctate colocalized with eGFP immunostaining (B1, arrow heads) did not  
926 colocalize with calbindin immunostaining (B2, arrow head). Barred arrow (B1) shows a  
927 colocalization of calbindin and synaptophysin immunostaining not apposed to eGFP  
928 immunostaining. B4) superimposed images (B1, B2 and B3) with z projections showing  
929 calbindin immunostaining and eGFP appositions. C1) Confocal stacks showing neurobiotin  
930 injected Foxd3 immunoreactive  $V1^R$ , HB9-eGFP immunostaining and synaptophysin  
931 immunostaining in an SC open book preparation. C2-C4). Single confocal sections with z  
932 projections of enlarged images from C1 (white box) showing the colocalization of

933 synaptophysin punctates with neurobiotin staining (C2), the apposition of the same  
934 synaptophysin punctates to eGFP (C3) and the apposition of neurobiotin staining containing  
935 synaptophysin punctates to eGFP (C4) (enlarged image in boxes in C2, C3 and C4),  
936 indicating the presence of a V1<sup>R</sup> synaptic-like contact on an MN neurite.

937

938 **Figure 4: Paracrine release of GABA detected by a sniffer outside-out patch.**

939 A1) Upper drawing showing the location of the outside-out sniffer to detect paracrine release  
940 of GABA (left) and to obtain outside-out currents in response to GABA application (left).

941 Lower traces (purple): example of outside-out sniffer current evoked by the application of 30  
942 mM KCl when the sniffer electrode was positioned in the dorsal area of the SC close to motor  
943 columns. Enlarged trace shows single channel currents at the onset of the sniffer current.

944 Right traces (green) show outside-out current evoked by the application of 3  $\mu$ M and 10  $\mu$ M  
945 GABA to a sniffer patch positioned outside the spinal cord. Purple and green traces are from  
946 the same outside-out patch. A2) Box plots of normalized maximum outside-out current

947 evoked by KCl application (purple left) and by the application of 3  $\mu$ M or 10  $\mu$ M GABA  
948 (green right) on the same outside-out sniffer patch (n = 9). Amplitudes of the outside-out  
949 currents evoked by the application of 30 mM KCl, 3  $\mu$ M or 10  $\mu$ M GABA, were normalized

950 to the amplitude of the outside-out currents evoked by the application of 30  $\mu$ M GABA (not  
951 shown). Note that the normalized amplitude of the outside-out current evoked by 30 mM KCl  
952 application ( $0.118 \pm 0.097$ ) was not significantly different ( $P > 0.9$ ) from the normalized

953 amplitude of the outside-out current evoked by the application of 3  $\mu$ M GABA ( $0.152 \pm$   
954  $0.062$ ). Normalized amplitudes of the outside-out currents evoked by the application of 30  
955 mM KCl or of 3  $\mu$ M GABA were significantly different (KCl:  $P = 0.0029$ ; 3  $\mu$ M GABA:  $P =$

956  $0.00665$ ) from the normalized amplitude of the outside-out currents evoked by the application  
957 of 10  $\mu$ M GABA ( $0.697 \pm 0.073$ ). V1<sup>R</sup>: immature Renshaw cell; MN: motoneuron; \*\*  $P <$   
958  $0.01$ . B1) Example of motoneuron membrane potential depolarization evoked by the

959 application of 3  $\mu\text{M}$  GABA in the presence of 1  $\mu\text{M}$  TTX (current clamp recording:  $V_h = -60$   
960 mV;  $E_{\text{Cl}} = -30$  mV). The application of 3  $\mu\text{M}$  GABA evoked a depolarizing response of  $20.6$   
961  $\pm 6.1$  mV ( $n = 7$ ).

962

963 **Figure 5:  $V1^{\text{R}}$  display plateau potential, repetitive firing or generate a single action**  
964 **potential during episodes of SNA in E12.5 spinal cord.**

965 Examples of spontaneous activities recorded in  $V1^{\text{R}}$  being characterized by GDPs displaying  
966 plateau potential (A), repetitive firing (B) or a single action potential (C) activity ( $V$  holding =  
967  $-60$  mV). Recordings shown in A, B and C are from different cells.

968

969 **Figure 6:  $V1^{\text{R}}$  display different excitability patterns in E12.5 embryonic spinal cords.**

970 Excitability patterns were analyzed using depolarizing current step (2 sec) and depolarizing  
971 current ramp (20 sec). A-D) Representative traces of voltage responses showing single-  
972 spiking activity (A), plateau potential activity (B) repetitive AP firing (C) and mixed  
973 repetitive-spiking/plateau potential activity (D). E) Proportions of  $V1^{\text{R}}$  subtypes according to  
974 the observed discharge patterns. 28.6% of  $V1^{\text{R}}$  could not sustain repetitive spiking, 41.7%  
975 were repetitive-spiking  $V1^{\text{R}}$ , 8.5% were mixed  $V1^{\text{R}}$ , 21.2% were plateau potential  $V1^{\text{R}}$  ( $n =$   
976 164). F) Plateau potentials are blocked by TTX (1  $\mu\text{M}$ ) application ( $n = 5/5$ ) (F1, F2). F2)  
977 Plateau potentials are evoked by short (100 ms) pulses of depolarizing current.

978

979 **Figure 7: Persistent sodium current ( $I_{\text{Nap}}$ ) is already expressed in  $V1^{\text{R}}$**

980 A1) Representative trace of  $I_{\text{Nap}}$  evoked by a slow depolarizing voltage ramp in a  $V1^{\text{R}}$  (CsCl  
981 intracellular solution).  $I_{\text{Nap}}$  (black trace) was isolated by subtracting the current elicited by a  
982 voltage ramp (70 mV/s) in the presence of TTX (insert green trace) from the control current  
983 (insert black trace). TTX-sensitive current was blocked by 5  $\mu\text{M}$  riluzole (red trace). Left  
984 insert shows the protocol to generate voltage-dependent slow inward currents in control

985 conditions (black), after 5  $\mu\text{M}$  riluzole application (red) or 1  $\mu\text{M}$  TTX application (green).  
 986 Right insert shows the current evoked by a depolarizing voltage step from -100 mV to 20 mV  
 987 in the absence and in the presence of 5  $\mu\text{M}$  riluzole. A2) Voltage dependence of  $I_{\text{Nap}}$   
 988 conductance calculated from the trace shown in A1. The activation curve was obtained by  
 989 transforming the current evoked by a depolarizing voltage ramp from -100 mV to 20 mV (70  
 990 mV/s) using the following equation:  $G_{\text{Nap}} = -I_{\text{Nap}}/((-V_h)+E_{\text{Na}^+})$  where  $V_h$  is the holding  
 991 potential at time  $t$  during a depolarizing voltage ramp and  $E_{\text{Na}^+}$  is the equilibrium potential for  
 992 sodium ( $E_{\text{Na}^+} = 60$  mV). The  $G_{\text{Nap}}/V_h$  curve was fitted with a Boltzmann function (see  
 993 methods), where  $V_{\text{half}}$  is the  $V_h$  value for  $I_{\text{Nap}}$  half activation,  $k$  the slope factor of the curve  
 994 and  $G_{\text{max}}$  the maximum conductance. B) Box plot showing  $G_{\text{max}}$  density in RCs ( $n=12$ ). C)  
 995 Box plots showing the variation of the %  $I_{\text{Nap}}$  block by 5  $\mu\text{M}$  riluzole in RC.

996

997 ***Figure 8: Effect of 5 and 10  $\mu\text{M}$  riluzole on action potentials.***

998 A) Effect of 5  $\mu\text{M}$  (red trace) and 10  $\mu\text{M}$  (blue trace) riluzole on the action potential (AP)  
 999 evoked by a depolarizing current step in an MN. B1) Box plot showing the % changes in AP  
 1000 amplitude (% of control) in the presence of 5  $\mu\text{M}$  riluzole and 10  $\mu\text{M}$  riluzole. B2) Box plot  
 1001 showing the % changes in AP threshold (% of control) in the presence of 5  $\mu\text{M}$  and 10  $\mu\text{M}$   
 1002 riluzole. B3) Box plot showing the % changes in AP half-width (% of control) in the presence  
 1003 of 5  $\mu\text{M}$  and 10  $\mu\text{M}$  riluzole.

1004

1005 ***Figure 9: Sustained discharge in embryonic  $V1^{\text{R}}$  depends on persistent sodium current***  
 1006 ***( $I_{\text{Nap}}$ ).***

1007 A) Representative traces of  $I_{\text{Nap}}$  recorded in  $V1^{\text{R}}$  that cannot sustain repetitive spiking (SS-  
 1008  $V1^{\text{R}}$ ) (A1), in a repetitive-spiking  $V1^{\text{R}}$  (RS- $V1^{\text{R}}$ ) (A2) and in a plateau potential  $V1^{\text{R}}$  (PP-  
 1009  $V1^{\text{R}}$ ) (A3).  $I_{\text{Nap}}$  was isolated by subtracting the current elicited by a slow voltage ramp (-100  
 1010 to + 20 mV; 70 mV/s) in the presence of 1  $\mu\text{M}$  TTX from the current evoked in the absence of

1011 TTX. A4) Box plots showing Gmax density in SS-V1<sup>R</sup> (n=13), RS-RCs (n=8) and PP-V1<sup>R</sup> (n  
1012 = 11). Note that Gmax density is significantly lower in SS-V1<sup>R</sup> (p <0.01). B) Representative  
1013 traces showing the effect of riluzole application (5  $\mu$ M) on the intrinsic activity pattern  
1014 evoked by suprathreshold current steps (left traces) or a suprathreshold current ramp (right  
1015 traces) in an RS-V1<sup>R</sup>. Note that riluzole blocks repetitive spiking (n= 10/10). C)  
1016 Representative traces showing the effect of riluzole application on plateau potential evoked by  
1017 suprathreshold current steps (left traces) or by a suprathreshold current ramp (right traces) in a  
1018 V1<sup>R</sup>. Note that riluzole blocks plateau potential activity (n=7/7).

1019

1020 ***Figure 10: Riluzole dramatically decreases the frequency and duration of episodes of SNA***  
1021 ***in E12.5 embryonic spinal cord.***

1022 A1) Application of 5  $\mu$ M riluzole inhibits spontaneous giant inward current (GIC) activity in  
1023 MNs (voltage clamp recordings; V<sub>h</sub> = -60 mV; ECl = -30 mV). A2) Enlarged trace from (A1)  
1024 showing GIC before (1, black) and at the onset of riluzole application (2, red). Note that the  
1025 amplitude and the duration of GICs were decreased on riluzole application. B1: Box plots  
1026 showing the amplitude of the GIC in a control and on riluzole application (n=8). B2: Box  
1027 plots showing half amplitude durations of the GIC in control and on riluzole application  
1028 (n=8). Note that the amplitude (P < 0.05) and the duration (P < 0.01) of GICs were  
1029 significantly reduced in the presence of riluzole. C) Spontaneous network activity (SNA)  
1030 recorded at the cervical (C) and lumbar (L) levels (see schematic drawing on the left) in  
1031 extracellular configuration before (C1) and after 5  $\mu$ M riluzole (C2). Note that one episode  
1032 still occurred 35 minutes after riluzole application. C3-C6) Box plots illustrating inter-burst  
1033 interval, burst duration, intra-burst spike frequency and cervical-lumbar delay of episode  
1034 propagation.

1035

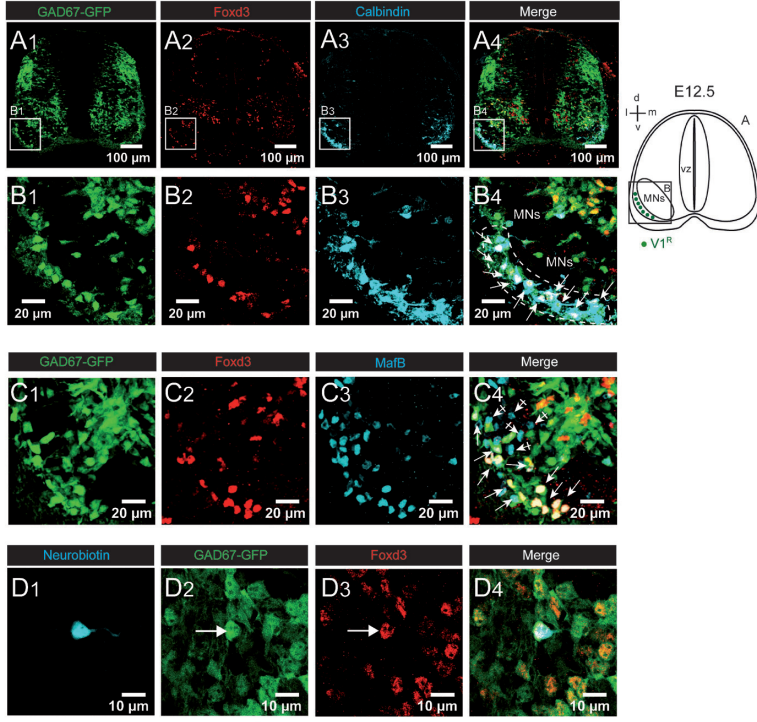
1036 **Table 1 Primary antibodies.**

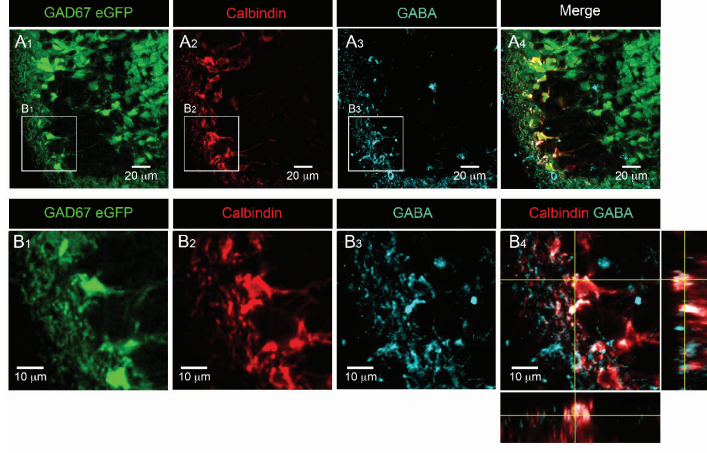


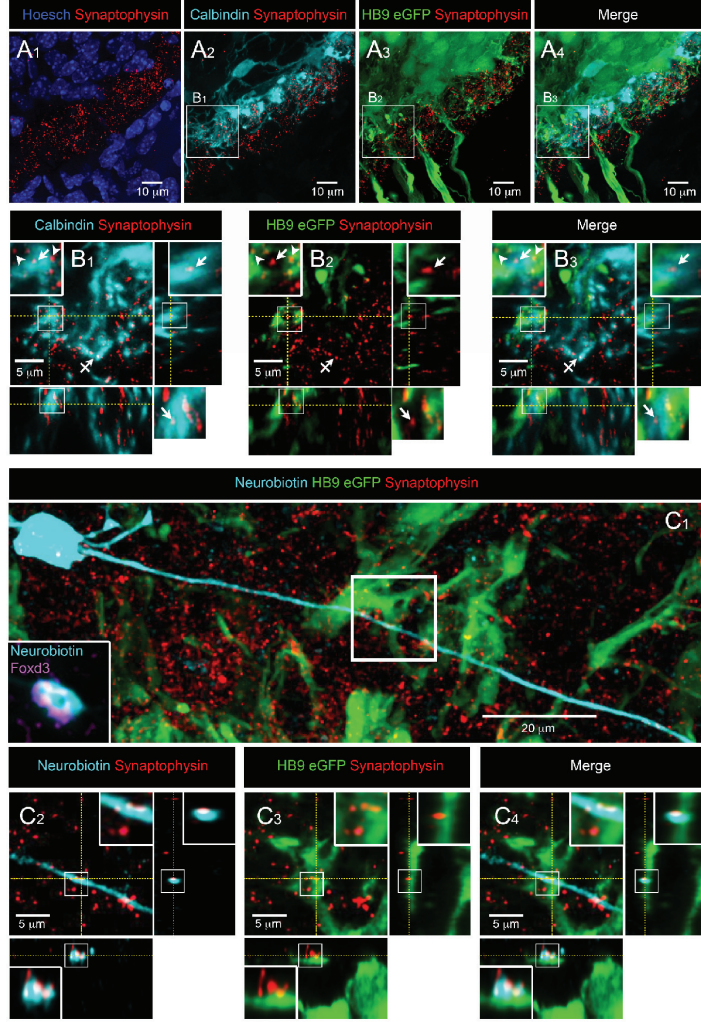
1037

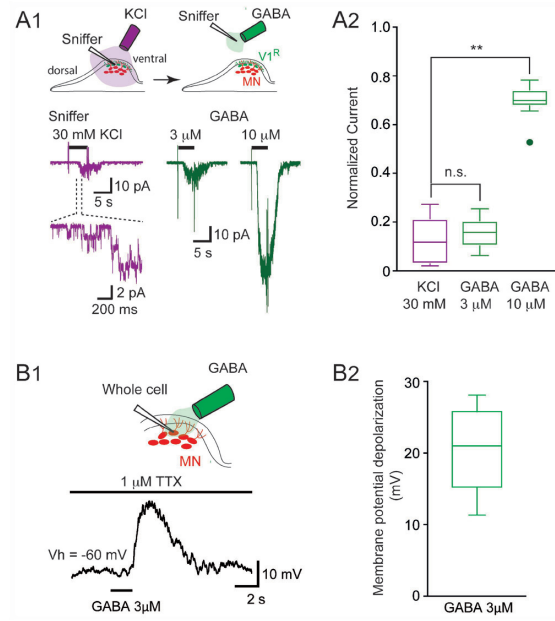
1038 **Table 2: Intrinsic membrane properties of Renshaw cells.**

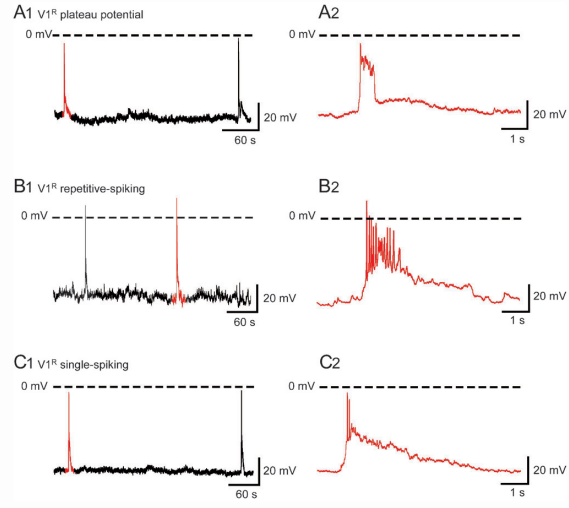
1039 SS-V1<sup>R</sup>: single-spiking Renshaw cells, RS-V1<sup>R</sup>: repetitive-spiking Renshaw cells, PP-V1<sup>R</sup>:  
1040 plateau potential Renshaw cells. AP: action potential. Threshold values represent the averaged  
1041 action potential threshold for single spiking V1<sup>R</sup> and repetitive spiking V1<sup>R</sup> and the averaged  
1042 plateau potential threshold for plateau potential V1<sup>R</sup>. Peak amplitude values represent the  
1043 averaged peak amplitude of the action potential for single spiking V1<sup>R</sup>, the averaged peak  
1044 amplitude of the first action potential in a train for repetitive spiking V1<sup>R</sup> and the averaged  
1045 peak amplitude of plateau potentials for plateau potential V1<sup>R</sup>. Half width values represent the  
1046 averaged half width of the action potential for single spiking V1<sup>R</sup>, the averaged half width of  
1047 the first action potential in a train for repetitive spiking V1<sup>R</sup> and the averaged half width of  
1048 plateau potentials for plateau potential V1<sup>R</sup>. Rate of rise values represent the averaged rate of  
1049 rise of the action potential for single spiking V1<sup>R</sup>, the averaged rate of rise of the first action  
1050 potential in a train for repetitive spiking V1<sup>R</sup> and the averaged rate of rise of plateau potentials  
1051 for plateau potential V1<sup>R</sup>. Values are expressed as mean  $\pm$  SD. Input resistance of SS-V1<sup>R</sup>,  
1052 input resistance of RS-V1<sup>R</sup> and input resistance of PP-V1<sup>R</sup> were not significantly different ( $P$   
1053 = 0.17).

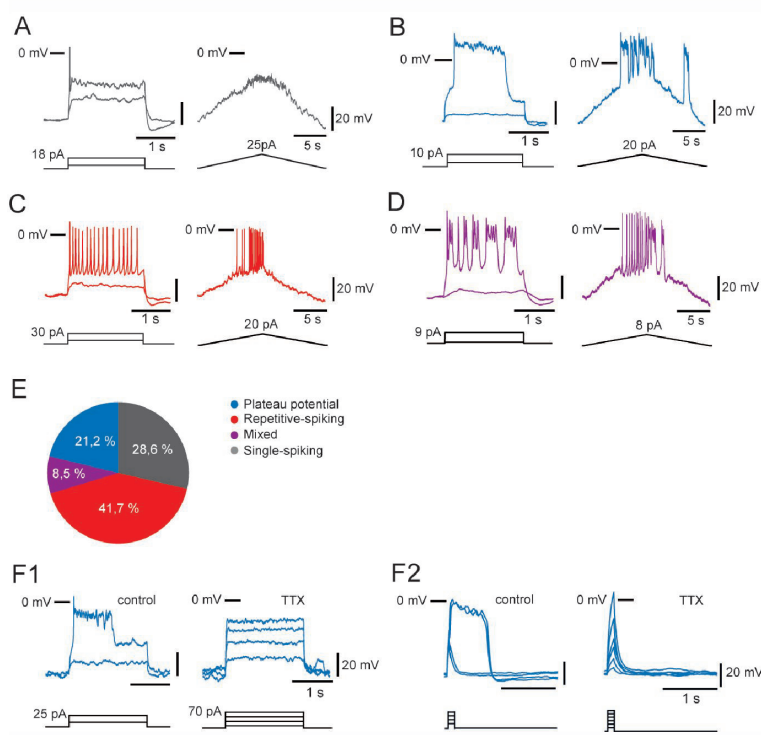


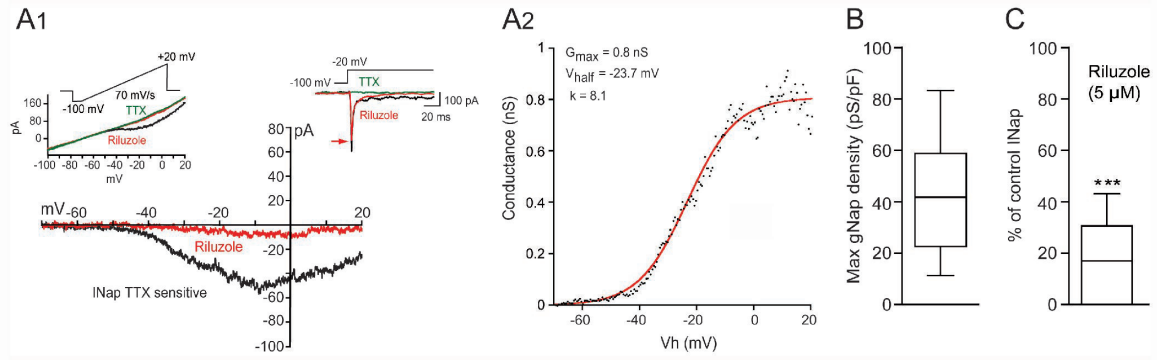




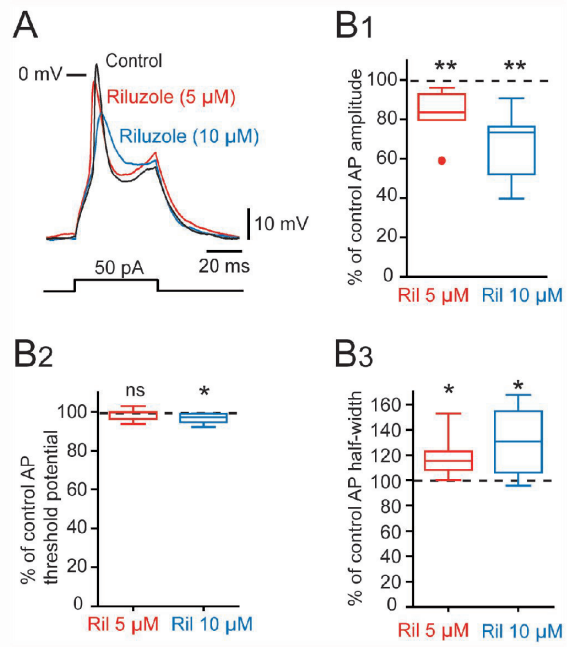


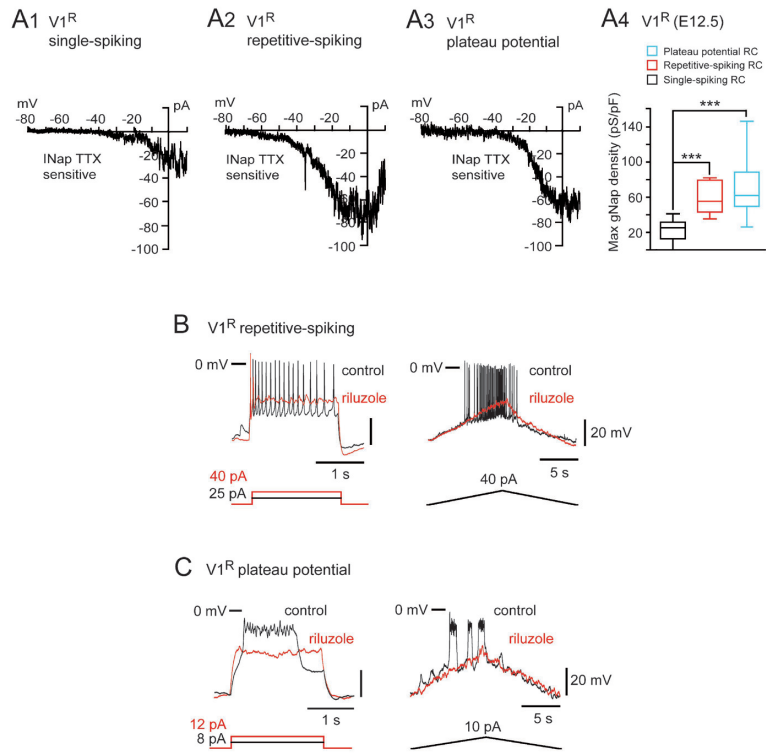












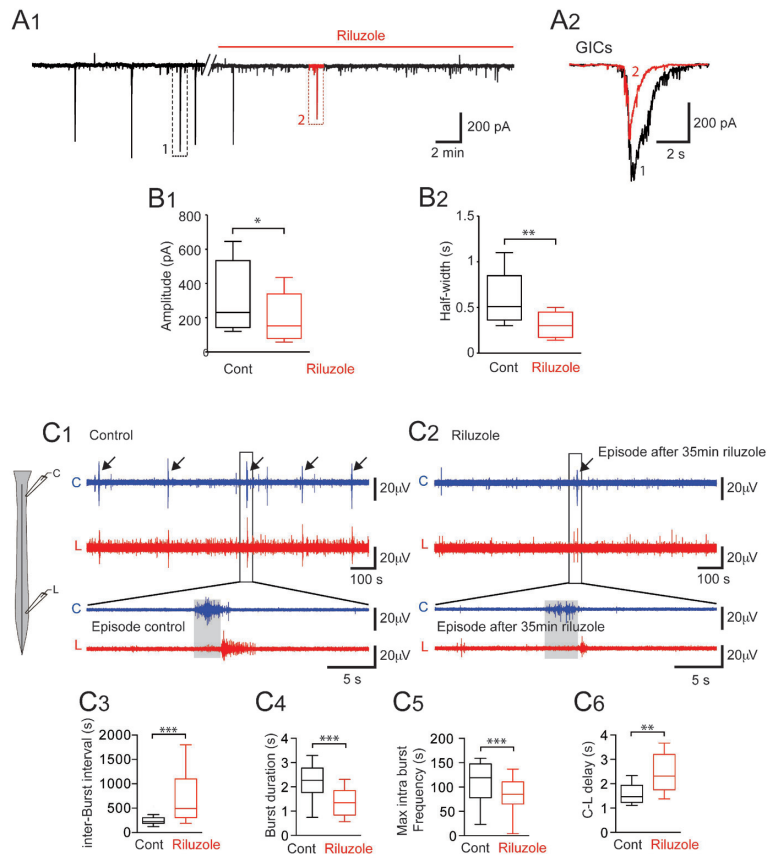


Table 1. Primary antibodies

Primary antibody	Company	Reference	Host/isotype	Dilution
anti-calbindin-D <sub>28k</sub>	Swant, Switzerland	(Swant Cat# CB38, RRID:AB_2721225)	Rabbit polyclonal	1:1500
anti-FoxD3	provided by C.Birchmeier, MDC Berlin, Germany	Storm R, et al.(2009) Development. ;136:295–305.	Guinea pig polyclonal	1:5000
anti-MafB	Bethyl Laboratories	Bethyl Cat# IHC-00351, RRID:AB_1279487	Rabbit polyclonal	1:1000
anti-GABA	Sigma-Aldrich	Sigma-Aldrich Cat# A0310, RRID:AB_476667	Mouse monoclonal	1:800
Anti-synaptophysin	Synaptic System	Synaptic Systems Cat# 101 011, RRID:AB_887824	Mouse monoclonal	1:1500
Anti-GFP	Aves Labs	Aves Labs Cat# GFP-1020, RRID:AB_10000240)	Chicken polyclonal	1 :1000

	Single-spiking V1 <sup>R</sup> (SS)	Repetitive- spiking V1 <sup>R</sup> (RS)	Plateau potential V1 <sup>R</sup> (PP)
Whole cell capacitance (pF)	13.3 ± 2.8 N = 82	15.3 ± 4.5 N = 60	12.4 ± 3.6 N = 50
Input resistance (MOhm)	1298 ± 682 N = 82	1156 ± 616 N = 60	1254 ± 508 N = 50
Threshold (mV)	-34.1 ± 3.3 N = 46	-33.6 ± 4.9 N = 53	-35.9 ± 6.0 N = 36
peak amplitude (mV)	-6.8 ± 6.1 N = 46	3.2 ± 6.7 N = 53	3.4 ± 10.3 N = 36
half width (ms)	11.2 ± 8.2 N = 46	12.8 ± 6.9 N = 53	705.7 ± 631.7 N = 36
rate of rise (mV/ms)	8.4 ± 3.8 N = 27	13.4 ± 9.4 N = 27	6.2 ± 3.7 N = 19

**Table 2: Intrinsic functional properties of V1<sup>R</sup>.**

SS-V1<sup>R</sup>: single-spiking Renshaw cells, RS-V1<sup>R</sup>: repetitive-spiking Renshaw cells, PP-V1<sup>R</sup>: plateau potential Renshaw cells. AP: action potential. Threshold values represent the averaged action potential threshold for single spiking V1<sup>R</sup> and repetitive spiking V1<sup>R</sup> and the averaged plateau potential threshold for plateau potential V1<sup>R</sup>. Peak amplitude values represent the averaged peak amplitude of the action potential for single spiking V1<sup>R</sup>, the averaged peak amplitude of the first action potential in a train for repetitive spiking V1<sup>R</sup> and the averaged peak amplitude of plateau potentials for plateau potential V1<sup>R</sup>. Half width values represent the averaged half width of the action potential for single spiking V1<sup>R</sup>, the averaged half width of the first action potential in a train for repetitive spiking V1<sup>R</sup> and the averaged half width of plateau potentials for plateau potential V1<sup>R</sup>. Rate of rise values represent the averaged rate of

rise of the action potential for single spiking  $V1^R$ , the averaged rate of rise of the first action potential in a train for repetitive spiking  $V1^R$  and the averaged rate of rise of plateau potentials for plateau potential  $V1^R$ . Values are expressed as mean  $\pm$  SD. Input resistance of SS- $V1^R$ , input resistance of RS- $V1^R$  and input resistance of PP- $V1^R$  were not significantly different ( $P = 0.17$ ).